

1
2
3
4
5
6
7
8
9
10
11
12
13
14
15
16
17
18
19
20
21
22

The organic sea surface microlayer in the upwelling region off
Peru and potential implications for air-sea exchange processes

Anja Engel* and Luisa Galgani

GEOMAR – Helmholtz Centre for Ocean Research Kiel, Düsterbrooker Weg 20,
24105 Kiel, Germany

* aengel@geomar.de, tel. +49 431 6001510

23 **Abstract:** The sea surface microlayer (SML) is at the very surface of the ocean, linking the
24 hydrosphere with the atmosphere. The presence and enrichment of organic compounds in the
25 SML have been suggested to influence air-sea gas exchange processes as well as the emission of
26 primary organic aerosols. Here, we report on organic matter components collected from an
27 approximately 50 μ m thick SML and from the underlying water (ULW), ~20 cm below the SML,
28 in December 2012 during the SOPRAN METEOR 91 cruise to the highly productive, coastal
29 upwelling regime off Peru. Samples were collected at 37 stations including coastal upwelling
30 sites and off-shore stations with less organic matter and were analyzed for total and dissolved
31 high molecular weight (>1kDa) combined carbohydrates (TCCHO, DCCHO), free amino acids
32 (FAA), total and dissolved hydrolysable amino acids (THAA, DHAA), transparent exopolymer
33 particles (TEP), Coomassie stainable particles (CSP), total and dissolved organic carbon (TOC,
34 DOC), total and dissolved nitrogen (TN, TDN), as well as bacterial and phytoplankton
35 abundance. Our results showed a close coupling between organic matter concentrations in the
36 water column and in the SML for almost all components except for FAA and DHAA that showed
37 highest enrichment in the SML on average. Accumulation of gel particles, i.e. TEP and CSP, in
38 the SML differed spatially. While CSP abundance in the SML was not related to wind speed,
39 TEP abundance decreased with wind speed, leading to a depletion of TEP in the SML at about 5
40 m s⁻¹. Our study provides insight to the physical and biological control of organic matter
41 enrichment in the SML, and discusses the potential role of organic matter in the SML for air-sea
42 exchange processes.

43

44

45

46

47 **1. Introduction**

48
49 The sea-surface microlayer (SML) is the uppermost layer of the water-column and the interface
50 between the ocean and the atmosphere. The accumulation of organic matter, distinct physical and
51 chemical properties and a specific organismal community (neuston) distinguish the SML as a
52 unique biogeochemical and ecological system. It has been suggested that the SML has a gel-like
53 nature (Cunliffe and Murrell, 2009; Sieburth, 1983) of varying thickness (20-150 μm , Cunliffe et
54 al., 2013) with dissolved polymeric carbohydrates and amino acids present as well as gel
55 particles, such as transparent exopolymer particles (TEP) of polysaccharidic composition, and
56 Coomassie stainable particles (CSP) of proteinaceous composition. These gelatinous compounds
57 originate from high molecular weight polymers that are released from phytoplankton and
58 bacterial cells by exudation and cell break up (Chin et al., 1998; Engel et al., 2004; Verdugo et
59 al., 2004). Polysaccharide-rich gels, like TEP, were attributed mainly to phytoplankton exudation
60 (Passow, 2002), while the production of protein-containing gels, such as CSP, has been related to
61 cell lysis and decomposition, as well as to the absorption of proteins onto non-proteinaceous
62 particles (Long and Azam, 1996). Gels are transported to the SML by rising bubbles (Azetsu-
63 Scott and Passow, 2004; Zhou et al., 1998) or are produced from dissolved precursors directly at
64 the air-sea interface during surface wave action (Wurl et al., 2011). Gel particles can promote
65 microbial biofilm formation (Bar-Zeev et al., 2012) and mediate vertical organic matter transport,
66 either to the atmosphere (Leck and Bigg, 2005; Orellana et al., 2011) or to the deep ocean
67 (Passow, 2002).

68
69 Accumulation of organic matter in the SML may be tightly coupled to phytoplankton abundance
70 in the water-column (Bigg et al., 2004; Galgani et al., 2014; Gao et al., 2012; Matrai et al., 2008).

71 Thus, organic matter accumulation and composition in the SML may also reflect the sensitivity of
72 marine microorganisms in the surface ocean to environmental changes, which was shown during
73 previous mesocosms studies (Engel et al., 2013; Riebesell et al., 2009; Schulz et al., 2013).
74 Distinct from the SML and on top of it lies the nanolayer, a monomolecular film, which, like the
75 SML, shows seasonality features with carbohydrate-rich polymeric material being most abundant
76 during the summer months and possibly related to a combination of primary production
77 (phytoplankton abundance) and photochemical and/or microbial reworking of organic matter
78 (Laß et al., 2013).

79 In our study we focused on the upper micrometers of the water-air interface that we operationally
80 defined as SML, whose compositional changes and accumulation of organic matter may
81 influence two air-sea interface processes necessary to understand oceanic feedbacks on the
82 atmosphere: sea-spray aerosol (SSA) emission and air-sea gas exchange (Cunliffe et al., 2013).
83 During biologically productive periods, a high amount of SSA with a predominant organic
84 composition is emitted from the ocean's surface (O'Dowd et al., 2004). These compounds
85 primarily reveal a polysaccharidic, gel-like composition, suggesting that the abundance and size
86 of dissolved polysaccharides and marine gels in the sea surface may influence the organic
87 fraction of SSA (Orellana et al., 2011; Russell et al., 2010). It has also been shown that the
88 presence of biogenic surface active substances (surfactants) in the SML leads to capillary wave
89 damping and alter the molecular diffusion of gases (Frew et al., 1990; Liss and Duce, 2005) and
90 therewith affects gas exchange rates particularly at lower wind speed (Jähne and Haußecker,
91 1998). In this respect, the understanding of sources, composition and fate of biological
92 components in the surface layer becomes of particular relevance for environments, where
93 biological productivity is high like in coastal upwelling regimes.

94 Off Peru, the coastal upwelling region extends between approximately 4°S and 40°S. In this area,
95 upwelling processes are sustained by winds throughout the year but feature high inter-annual
96 variability induced by the El Niño-Southern Oscillation (ENSO) cycle (Tarazona and Arntz,
97 2001). Eastern Boundary Upwelling Systems (EBUS's) like the system off Peru are characterized
98 by high biological productivity supported by deep upwelling of nutrients and often associated
99 with subsurface Oxygen Minimum Zones (OMZ's). The supply of oxygen to the OMZ is largely
100 controlled by physical, i.e. diffusive and advective, mechanisms, whereas biological processes,
101 i.e. respiration of organic matter, provide sinks (Lachkar and Gruber, 2011).

102 OMZ's are significant source regions for major climate relevant gases such as carbon dioxide,
103 methane, hydrogen sulfide and nitrous oxide (Paulmier et al., 2008; Paulmier et al., 2011).
104 Processes affecting gas exchange in these regions need to be understood in order to accurately
105 estimate trace gas fluxes from the ocean to the atmosphere and consequences on climate. In 2008,
106 the VAMOS Ocean-Cloud-Atmosphere-Land Study Regional Experiment (VOCALS-REx) and
107 the Chilean Upwelling Experiment (VOCALS-CUpEx) conducted between Southern Peru and
108 Northern Chile focused on the link between aerosols, clouds and precipitation as well as on
109 physical and chemical couplings between the upper ocean and the lower atmosphere (Garreaud et
110 al., 2011; Wood et al., 2011). During the SOPRAN cruise METEOR91 (M91), we studied
111 organic matter components at the very sea surface since properties of the SML may represent a
112 major uncertainty for gas, heat and aerosol fluxes in this specific region and in other oceanic
113 environments. During our cruise, organic matter concentration and composition of the SML and
114 the underlying seawater were studied on 37 different stations, providing the first SML data-set for
115 the upwelling system off Peru, including the first data-set on gel particles in EBU's so far.

117
118 **2. Material and Methods**
119
120 **2.1. Field information and sampling**

121 The *R/V METEOR* cruise M91 studied the upwelling region off Peru (Bange, 2013). Samples
122 were collected between 4.59° S and 82.0°W, and 15.4°S and 77.5°W from December 03 to 23 in
123 2012. The overall goal of M91 was to conduct an integrated biogeochemical study on the
124 upwelling region off Peru in order to assess the importance of OMZ's for the sea-air exchange of
125 various climate-relevant trace gases and for tropospheric chemistry. Salinity and temperature
126 were measured with a CTD at each station. Global and UV radiation and wind speed data were
127 retrieved from the DShip database for the time of sampling based on the sensors installed on
128 board.

129 On 37 different stations between 5°S and 16°S off the Peruvian coast (Figure 1), a total of 39
130 SML samples was collected from a rubber boat using a glass plate sampler according to the
131 original approach described by Harvey and Burzell (1972). Different methods have been
132 developed to sample and investigate the SML. These methods do not only differ in terms of
133 application but also with respect to the thickness of the SML sampled as well as to selective
134 removal of certain components. Several studies evaluated these methods against each other. A
135 recent summary can be found in the 'Guide to best practices to study the ocean's surface'
136 (Cunliffe and Wurl, 2014). During this study, we applied the glass plate technique because it
137 allows for sampling of a relatively large volume needed to analyze different organic components
138 while keeping the simultaneous sampling of ULW minimal. Two stations were sampled twice in
139 a time frame of 24 hours (stations 12_1 and 12_3, 16_2 and 16_3). Our glass plate with the
140 dimensions of 500 mm (length) x 250 mm (width) x 5 mm (thickness) was made of borosilicate
141 glass and had an effective sampling surface area of 2000 cm² (considering both sides). For each
142 sample, the glass plate was inserted into the water perpendicular to the surface and withdrawn

143 slowly at a rate of approximately 20 cm sec^{-1} . The sample, retained on the glass because of
144 surface tension, was removed with the help of a Teflon wiper. Samples were collected as far
145 upwind of the ship as possible and away from the path taken by the ship to avoid contamination.
146 For each sample the glass plate was dipped and wiped about twenty times. The exact number of
147 dips and the total volume collected were recorded. Samples were collected into acid cleaned
148 (HCl, 10%) and Milli-Q washed glass bottles, and the first milliliters were used to rinse the
149 bottles and then discarded. Prior to each sampling, both glass plate and wiper were washed with
150 HCl (10%) and intensively rinsed with Milli-Q water. At the sampling site, both instruments were
151 copiously rinsed with seawater in order to minimize any possible contamination with alien
152 material while handling or transporting the devices.

153 The apparent thickness (d) of the layer sampled with the glass plate was determined as follows:

154 (1)
$$d = V / (A \times n)$$

155 Where V is the SML volume collected, i.e. 60-140 mL, A is the sampling area of the glass plate
156 ($A = 2000 \text{ cm}^2$) and n is the number of dips (Cunliffe and Wurl, 2014). We will use d (μm) as an
157 operational estimate for the thickness of the SML.

158 At the same stations, after sampling the SML, about 500 mL samples were collected from the
159 underlying seawater (ULW) at $\sim 20 \text{ cm}$ depth by holding an acid cleaned (HCl 10%) and Milli-Q
160 rinsed borosilicate glass bottle. The bottle was open and closed underwater to avoid simultaneous
161 sampling of SML water. For safety reasons sampling for the SML from a rubber boat could be
162 made only during daylight hours.

163

164 **2.2 Chemical and biological analyses**

165 **2.2.1. Total organic carbon (TOC) and dissolved organic carbon (DOC)**

166 Samples for TOC and DOC (20 ml) were collected in combusted glass ampoules, DOC after
167 filtration through combusted GF/F filters (8 hours, 500° C). Samples were acidified with 80 µL of
168 85% phosphoric acid, heat sealed immediately, and stored at 4°C in the dark until analysis. DOC
169 and TOC samples were analyzed by applying the high-temperature catalytic oxidation method
170 (TOC -VCSH, Shimadzu) modified from Sugimura and Suzuki (1988). The instrument was
171 calibrated every 8-10 days by measuring standard solutions of 0, 500, 1000, 1500, 2500 and 5000
172 µg C L⁻¹, prepared from a potassium hydrogen phthalate standard (Merck 109017). Every
173 measurement day, ultrapure (MilliQ) water was used to determine the instrument blank, which
174 was accepted for values <1 µmol C L⁻¹. TOC analysis was validated on every measurement day
175 with deep seawater reference (DSR) material provided by the Consensus Reference Materials
176 Project of RSMAS (University of Miami) yielding values within the certified range of 42-45
177 µmol C L⁻¹. Additionally, two internal standards with DOC within the range of those in samples
178 were prepared each measurement day using a potassium hydrogen phthalate (Merck 109017).
179 DOC and TOC concentration was determined in each sample from 5 to 8 injections. The
180 precision was <4% estimated as the standard deviation of replicate measurements divided by the
181 mean. Particulate organic carbon (POC) was determined as the difference between TOC and
182 DOC.

183 **2.2.2. Total nitrogen (TN) and total dissolved nitrogen (TDN)**

184 TN and TDN were determined simultaneously with TOC and DOC, respectively, using the TNM-
185 1 detector on the Shimadzu analyzer. Nitrogen in the samples is combusted and converted to
186 NO_x, which chemiluminesces when mixed with ozone and can be detected using a
187 photomultiplier (Dickson et al., 2007). Calibration of the instrument was done every 8-10 days
188 by measuring standard solutions of 0, 100, 250, 500 and 800 µg N L⁻¹, prepared with potassium
189 nitrate Suprapur® (Merck 105065). Particulate nitrogen (PN) was determined as the difference

190 between TN and TDN. Deep seawater reference (DSR) material provided by the Consensus
191 Reference Materials Project of RSMAS (University of Miami) was used on every measurement
192 day and yielded values within the certified range of 31-33 $\mu\text{mol N L}^{-1}$. The precision was <2%
193 estimated as the standard deviation of 5-8 measurements divided by the mean.

194

195 **2.2.3. Total, dissolved and free amino acids**

196 For total hydrolysable amino acids (THAA), 5 mL of sample were filled into pre-combusted glass
197 vials (8 hours, 500°C) and stored at -20 °C until analysis. Samples for dissolved hydrolysable
198 (DHAA) and free amino acids (FAA) were additionally filtered through 0.45 μm Millipore
199 Acrodisc® syringe filters and then stored in the same way as samples for THAA. Analysis was
200 performed according to Lindroth & Mopper (1979) and Dittmar et al. (2009) with some
201 modifications. Duplicate samples were hydrolyzed for 20h at 100°C with hydrochloric acid
202 (suprapur, Merck) and neutralized by acid evaporation under vacuum in a microwave at 60°C.
203 Samples were washed with water to remove remaining acid. Analysis was performed on a 1260
204 HPLC system (Agilent). Thirteen different amino acids were separated with a C18 column
205 (Phenomenex Kinetex, 2.6 μm , 150 x 4.6 mm) after in-line derivatization with o-phthaldialdehyde
206 and mercaptoethanol. The following standard amino acids were used: aspartic acid (AsX),
207 glutamic acid (GIX), serine (Ser), arginine (Arg), glycine (Gly), threonine (Thr), alanine (Ala),
208 tyrosine (Tyr), valine (Val), phenylalanine (Phe), isoleucine (Ileu), leucine (Leu), γ - amino
209 butyric acid (GABA). α - amino butyric acid was used as an internal standard to account for
210 losses during handling. Solvent A was 5% acetonitrile (LiChrosolv, Merck, HPLC gradient
211 grade) in sodium-di-hydrogen-phosphate (Merck, suprapur) Buffer (PH 7.0). Solvent B was
212 acetonitrile. A gradient was run from 100% solvent A to 78% solvent A in 50 minutes. FAA were
213 determined from DHAA samples without prior hydrolysis in separate analyses. Particulate

214 hydrolysable amino acids (PHAA) were determined by subtracting DHAA from THAA. The
215 detection limit for individual amino acids was 2 nmol monomer L⁻¹. The precision was <5%,
216 estimated as the standard deviation of replicate measurements divided by the mean.

217

218 **2.2.4. Total and dissolved combined carbohydrates**

219 For total and dissolved combined carbohydrates > 1 kDa (TCCHO and DCCHO), 20 mL were
220 filled into pre-combusted glass vials (8 hours, 500 °C) and kept frozen at -20 °C until analysis.
221 Samples for DCCHO were additionally filtered through 0.45 µm Pall Acrodisc® syringe filters.
222 The analysis was conducted according to Engel and Händel (2011) applying high performance
223 anion exchange chromatography coupled with pulsed amperometric detection (HPAEC-PAD) on
224 a Dionex ICS 3000. Samples were desalinated by membrane dialysis (1 kDa MWCO, Spectra
225 Por) for 5 h at 1 °C, hydrolyzed for 20 h at 100°C with 0.4 M HCl final concentration, and
226 neutralized through acid evaporation under vacuum and nitrogen atmosphere (1h, 60 °C) Two
227 replicate samples were analyzed. The retention of carbohydrates on exchange columns, and thus
228 the reproducibility of results are highly sensitive to changes in temperature (Panagiotopoulos et
229 al., 2001; Yu and Mou, 2006). For our system, best resolution of sugars was obtained at 25 °C
230 and therefore applied constantly during all analyses. In order to minimize degradation of samples
231 before analysis, the temperature in the auto-sampler was kept at 4 °C. The system was calibrated
232 with a mixed sugar standard solution including a) the neutral sugars: fucose (4.6 µM, Fuc),
233 rhamnose (3.1 µM, Rha), arabinose (2.0 µM, Ara), galactose (2.4 µM, Gal), xylose/ mannose (3.1
234 µM, Xyl/ Man), glucose (2.4 µM, Glc), b) the amino sugars: galactosamine (2.0 µM, GalN),
235 glucosamine (2.8 µM, GlcN), and c) the acidic sugars: galacturonic acid (2.8 µM, Gal-URA),
236 gluconic acid (5.1 µM, Glu-Ac), glucuronic acid (3.0 µM, Glc-URA) and muramic acid (1.9 µM,
237 Mur-Ac). Regular calibration was performed by injecting 12.5 µl, 15.0 µl, 17.5 µl and 20 µl of

238 mixed standard solution. Linearity of the calibration curves of individual sugar standards was
239 verified in the concentration range 10 nM-10 μ M. Therefore, the standard mixture was diluted
240 10, 20, 50, and 100 fold with Milli-Q water. Injection volume for samples and for the blank was
241 17.5 μ l. To check the performance of carbohydrate analysis and stability of the HPLC-PAD
242 system, a 17.5 μ l standard solution was analyzed after every second sample. The detection limit
243 was 10 nM for each sugar with a standard deviation between replicate runs of <2%. Milli-Q water
244 was used as blank to account for potential contamination during sample handling. Blanks were
245 treated and analyzed in the same way as the samples. Blank concentration was subtracted from
246 sample concentration if above the detection limit. Particulate combined carbohydrates (PCCHO)
247 were determined as the difference between TCCHO and DCCHO.

248

249 **2.2.5. Gel particles**

250 Total area, particle numbers and equivalent spherical diameter (d_p) of gel particles were
251 determined by microscopy after Engel (2009). Therefore, 20 to 30 mL were filtered onto 0.4 μ m
252 Nuclepore membranes (Whatmann) and stained with 1 mL Alcian Blue solution for
253 polysaccharidic gels, i.e. transparent exopolymer particles (TEP), and 1 mL Coomassie Brilliant
254 Blue G (CBBG) working solution for proteinaceous gels, i.e. Coomassie stainable particles
255 (CSP). Filters were mounted onto Cytoclear[®] slides and stored at -20 $^{\circ}$ C until microscopy
256 analysis. The size-frequency distribution of gel particles was described by:

257

$$258 \quad (2) \quad \frac{dN}{d(d_p)} = k d_p^{\delta}$$

259

260 where dN is the number of particles per unit water volume in the size range d_p to $(d_p + d(d_p))$
261 (Mari and Kiørboe, 1996). The factor k is a constant that depends on the total number of particles

262 per volume, and δ ($\delta < 0$) describes the spectral slope of the size distribution. The value δ is
 263 related to the slope of the cumulative size distribution $N = \alpha d_p^\beta$ by $\delta = \beta + 1$, where N is the total
 264 number of particles per unit water volume. The less negative is δ , the greater is the fraction of
 265 larger gels. Both δ and k were derived from regressions of $\log(dN/d(d_p))$ versus $\log(d_p)$ over the
 266 size range 1.05-14.14 μm ESD.

267 Formation of exopolymeric gel particles, e.g. TEP, can be described in terms of coagulation
 268 kinetics (Engel et al., 2004; Mari and Burd, 1998). Aggregates can be described using a fractal
 269 scaling relationship, e.g. $M \sim L^D$, where M is the mass of the aggregate, L the size and D is the
 270 fractal dimension, which is controlled by the size of particles that form the aggregate as well as
 271 by the processes of particle collision, e.g. Brownian Motion, shear, or differential settlement
 272 (Meakin, 1991). Assuming that TEP are formed by shear induced coagulation D can be estimated
 273 from δ (Mari and Burd, 1998):

274

$$275 \quad (3) \quad D = \frac{(64 - \delta)}{26.2}$$

276

277 **2.2.6. Heterotrophic bacteria**

278 For bacterial cell numbers, 4 mL samples were fixed with 200 μL glutaraldehyde (25% final
 279 concentration) and stored at -20°C until enumeration. Samples were stained with SYBR Green I
 280 (Molecular Probes). Heterotrophic bacteria were enumerated using a flow cytometer (Becton &
 281 Dickinson FACScalibur) equipped with a laser emitting at 488 nm and detected by their signature
 282 in a plot of side scatter (SSC) versus green fluorescence (FL1). Heterotrophic bacteria were
 283 distinguished from photosynthetic prokaryotes (e.g. *Prochlorococcus*) by their signature in a plot
 284 of red fluorescence (FL2) versus green fluorescence (FL 1). Yellow-green latex beads

285 (Polysciences, 0.5 μm) were used as internal standard. Sampling bacterioneuston with a glass
286 plate does not bias cell abundance measurements (Stolle et al., 2009).

287

288 **2.2.7. Phytoplankton**

289 For photoautotrophic cell numbers $<20 \mu\text{m}$, 4 mL samples were fixed with 20 μL glutaraldehyde
290 (25% final concentration), and stored at -80°C until enumeration. Phytoplankton counts were
291 performed with a FACSCalibur flow-cytometer (Becton Dickinson) equipped with an air-cooled
292 laser providing 15 mW at 488 nm and with a standard filter set-up. The cells were analyzed at
293 high flow rate ($\sim 39\text{-}41 \mu\text{L min}^{-1}$) with the addition of $1\mu\text{m}$ -fluorescent beads (Trucount, BD).
294 Autotrophic groups were discriminated on the basis of their forward or right angle light scatter
295 (FALS, RALS) as well as from chlorophyll and phycoerythrin (characteristic for cyanobacterial,
296 mainly *Synechococcus* populations) fluorescence. Cell counts were analyzed using BD CellQuest
297 Pro-Software. Two groups were distinguished: Non-cyanobacterial-type phytoplankton (NCPL)
298 and cyanobacterial-type phytoplankton (CPL).

299

300 **2.3. Data analysis**

301 The relative concentration of a substance A in the SML was compared to the underlying water
302 (ULW) by the enrichment factor (EF), defined by:

$$303 \quad (4) \quad EF = (A)_{\text{SML}} / (A)_{\text{ULW}}$$

304 Where (A) is the concentration of a given parameter in the SML or ULW, respectively
305 (GESAMP, 1995). Because the concentration of a component is normalized to its values in the
306 underlying water, EF for different components can be readily compared. Enrichment of a
307 component is indicated by $EF > 1$, depletion by $EF < 1$.

308

309 Differences in data as revealed by statistical tests (*t*-test) were accepted as significant for $p < 0.05$.
310 Average values for total concentrations are given by their arithmetic mean, averages for ratios by
311 their geometric mean. Average values are reported with ± 1 standard deviation (SD). Calculations,
312 statistical tests and illustration of the data were performed with the software packages Microsoft
313 Office Excel 2010, Sigma Plot 12.0 (Systat) and Ocean Data View (Schlitzer, 2013). Weighted-
314 average gridding was used in ODV to display data in the SML according to data coverage with
315 automatic scale lengths (53 permille x-scale length, 40 permille y-scale length).

316
317

318 **3. Results**

319

320 **3.1. The physical environment**

321

322 Coastal upwelling off Peru can occur throughout the year (Carr and Kearns, 2003). During the
323 M91 cruise upwelling and upwelling velocities were determined from $^3\text{He}/^4\text{He}$ disequilibrium
324 (Steinfeldt et al., 2015). High upwelling velocities of $>3 \times 10^{-5} \text{ m s}^{-1}$ were observed south of Lima
325 (stations 10, 14, 15) (Figure 1). The coastal upwelling of deep water resulted in strong gradients
326 of surface seawater temperature and salinity along the Peruvian shelf as well as with increasing
327 distance to the shelf during M91. Salinity measured at about 1 m depth corresponding to the
328 ship's keel varied between 32 and 35 with the lowest values occurring close to the coast at
329 stations 10_1 to 10_4, 14_1 and 14_2 and 15_1 to 15_3 Here, temperatures were below the
330 average of all surface stations ($19.25 \pm 1.7^\circ\text{C}$), indicating the colder, upwelling deep water (Table
331 1, Figure 2). Wind speed encountered during the cruise ranged between 0.6 and 9.0 m s^{-1} with the
332 lower wind speeds also observed closer to the coast, i.e. between 12° and 14°S and at the
333 northern stations (Figure 2). Thus, higher wind speed was observed at the more off-shore stations
334 having higher surface water temperatures, leading to significant co-variation between surface
335 water temperature and wind speed (Figure 3). Global radiation and UV radiation varied between

336 10 and 1103 W m⁻², and between 0.8 and 71 W m⁻², respectively, with no significant impact of
337 SML organic matter accumulation.

338

339 **3.2. SML properties and organic matter accumulation**

340 Estimates for SML thickness are depending on the method applied to sample the SML (Carlson,
341 1982; Zhang et al., 1998). For the glass plate technique, Zhang et al. (1998) showed that SML
342 thickness decreases with increasing withdrawal rates; i.e. from 50-60 µm for a withdrawal rate of
343 20 cm s⁻¹, to 10-20 µm at rate of 5-6 cm s⁻¹. Their results confirmed earlier studies that generally
344 revealed thinner SML layers at slower withdrawal rates (Carlson, 1982; Harvey and Burzell,
345 1972; Hatcher and Parker, 1974). During this study, the SML was sampled with the glass plate at
346 ~20 cm s⁻¹, yielding a thickness between 45 and 60 µm, with an overall mean value of 49± 8.89
347 µm (n=39). This value is in good accordance with the proposed apparent sampling thickness of
348 50±10 µm (Zhang et al., 1998) and fits well to previous observations for the SML sampled with a
349 glass plate at the same withdrawal rate (Cunliffe et al., 2011; Galgani and Engel, 2013; Galgani et
350 al., 2014; Zhang et al., 1998; Zhang, 2003). Using direct pH microelectrode measurements,
351 Zhang (2003) later confirmed an *in situ* thickness of ~60 µm for the SML, which they defined as
352 the layer of sudden change of physico-chemical properties.

353 We therefore assume that samples obtained from the SML during this study well represented the
354 SML, as defined by Zhang (2003). Thickness of the SML as determined during this study
355 increased significantly with amount of organic substances in the SML, determined as TOC
356 concentration ($p < 0.005$; $n = 39$). This corroborates earlier findings from experimental studies
357 showing that organic matter produced by phytoplankton increases the thickness of SML sampled
358 with a glass plate (Galgani and Engel, 2013). No correlation instead was observed between SML

359 thickness and wind speed ($r=-0.11$, $n=39$) or between SML thickness and temperature ($r=-0.06$;
360 $n=39$).

361
362 Unless stated otherwise, all observations described in this paragraph relate to the SML. In
363 general, concentration of organic components in the SML showed spatial distribution patterns
364 resembling those of temperature and wind speed (Figures 3, 4, 5). Highest concentration values
365 for nearly all organic components were observed at the upwelling stations 10_1 to 10_4, 14_1
366 and 14_2 and 15_1 to 15_3 (Figure 1) in accordance with high estimated primary production
367 rates (Steinfeldt et al., 2015) and high Chl *a* concentrations (Hu et al., 2015) determined in
368 surface waters at these sites during M91.

369 Phytoneuston abundances (<20 μm) varied between 3.7×10^3 and 1.9×10^5 mL^{-1} for
370 cyanobacterial-type phytoplankton (CPL) (mainly *Synechococcus spp.*) and between 5.4×10^3 and
371 3.0×10^5 mL^{-1} for other non-cyanobacterial-type phytoplankton (NCPL). Generally, highest
372 abundance was determined on and close to the upwelling stations (Figure 4). On all other
373 stations, cell abundance of CPL and NCPL differed spatially, with higher abundance of NCPL at
374 the southern stations and higher numbers of CPL at the northern stations (Figure 4). NCPL and
375 CPL were closely related to cell abundance in the ULW (Table 3).

376 Heterotrophic bacteria were determined in abundances between 3.0×10^4 and 8.5×10^6 mL^{-1}
377 with highest numbers observed at the upwelling stations and southeast of the upwelling (Figure
378 4). Heterotrophic bacteria in the SML were highly positively correlated to abundances in the
379 ULW ($r=0.94$; $n=36$ $p<0.001$) and negatively influenced by wind speed, although less clearly
380 ($r=-0.37$; $n=36$ $p=0.01$). No significant influence on heterotrophic bacteria abundance was
381 detected with respect to global radiation or UV radiation.

382 TOC concentration ranged between 82 and 199 $\mu\text{mol L}^{-1}$, and was clearly higher than
383 DOC concentration on all stations. Particulate Organic Carbon (POC) concentration was
384 calculated as the difference between TOC and DOC and ranged from 2.3 to 96 $\mu\text{mol L}^{-1}$. Highest
385 POC concentration was observed at the upwelling stations (Figure 5). In general, POC
386 concentration was highly correlated to temperature ($r=-0.67$, $n=39$ $p<0.001$) and to wind speed
387 ($r=-0.48$, $n=39$ $p<0.001$) (Table 3). DOC concentration ranged between 71 and 122 $\mu\text{mol L}^{-1}$
388 (Table 2) and, in contrast to POC, was not significantly related to temperature or wind speed
389 (Table 3). Relatively high DOC concentrations of about 100 $\mu\text{mol L}^{-1}$ were observed at stations 9
390 and 9_2 (Figure 5), but excluding these stations from analysis did not reveal a correlation to
391 temperature or wind speed either. DOC is a bulk measure and is quantitatively dominated by
392 refractory compounds that are independent from recent biological productivity. More closely
393 linked to productivity and likely stimulated by the upwelling of nutrients along the Peruvian coast
394 are labile and semi-labile compounds such as dissolved combined carbohydrates and amino acids.
395 Indeed, both DCCHO and DHAA reached highest concentrations at the upwelling stations
396 (Figure 5). Thereby, maximum concentration of DCCHO of 2670 nmol L^{-1} (mean: 1110 ± 550
397 nmol L^{-1}) was observed at station 15_2, slightly south of the station 14_1 exhibiting highest
398 DHAA concentrations of 2020 nmol L^{-1} (mean: 770 ± 360 nmol L^{-1}) (Table 2). In general high
399 DCCHO concentration was more focused to the upwelling, and exhibited strong horizontal
400 gradients to the northern and southern stations.

401 DHAA concentration was on average lower than DCCHO concentration (Table 2) and
402 horizontal differences were less pronounced than for DCCHO. Both components of semi-labile
403 DOC were inversely correlated to temperature (DCCHO $r=-0.44$, $n=39$, $p<0.001$; DHAA: $r=-$
404 0.47 , $n=30$, $p<0.001$), linking their accumulation in the SML to productivity in the cold
405 upwelling waters.

406 Concentrations of carbohydrates and amino acid in particles, and in gels (i.e. TEP, CSP) in
407 particular, were highest at the coastal upwelling stations also. Particulate carbohydrates and
408 amino acids (PCCHO, PHAA) were highly correlated to POC concentrations (PCCHO: $r=0.70$,
409 $n=39$, $p<0.001$; PHAA: $r=0.81$, $n=30$, $p<0.001$).

410 In general, numerical abundance as well as total area were about 10-fold higher for CSP
411 than for TEP (Table 2). Spatial variability of gel particles abundance was high, and yielded
412 lowest values of total TEP area of $6.9 \text{ mm}^2 \text{ L}^{-1}$ at station 13_1 and highest values of $408 \text{ mm}^2 \text{ L}^{-1}$
413 at station 15_1, about 100 nautical miles apart. The highest abundance of both TEP and CSP was
414 observed close to the coastal upwelling, but apart from these stations, the distribution of TEP in
415 the SML clearly differed from that of CSP (Figure 5). While higher TEP abundance was
416 observed at the northern stations, CSP abundance was more pronounced at the southern stations.
417 Moreover, stations of highest and lowest concentration of CSP were different from those of TEP.
418 Lowest value of CSP total area of $137 \text{ mm}^2 \text{ L}^{-1}$ was observed at station 11_1 and highest values
419 of $3051 \text{ mm}^2 \text{ L}^{-1}$ at station 14_1.

420

421 **3.3. Accumulation patterns in the SML**

422 For almost all components investigated during this study, concentration in the SML was
423 significantly related to the respective concentration in the ULW (Table 3). Thereby, correlations
424 between SML and ULW were strongest for combined carbohydrates, particularly for DCCHO.
425 Close correlations were also observed for bulk organic carbon measurements, i.e. TOC, DOC,
426 and derived therefrom POC. For dissolved nitrogenous compounds, i.e. TDN, FAA and DHAA
427 no relationship between SML and ULW concentrations was observed, suggesting that loss or
428 gain of these compounds in the SML were faster than exchange processes with the ULW.
429 Temperature had an effect on most organic compounds in the SML, with generally higher

430 concentrations at lower temperature (Table 3). This can largely be attributed to the higher
431 production of organic matter at the colder upwelling sites. Concentrations of particulate
432 components POC, TEP, PHCHO, PHAA and particulate nitrogen (PN) were also inversely
433 related to wind speed, whereas DCCHO and DHAA were inversely related to temperature but not
434 to wind speed. Clear differences were observed for the two different gel particle types determined
435 in this study. In contrast to TEP, neither abundance nor total area of CSP were related to wind
436 speed, nor to seawater temperature. Instead abundance of CSP in the SML was mostly related to
437 their abundance in ULW. However, with the exception of CSP, particulate components in the
438 SML were affected by changes in wind speed more than concentration of dissolved compounds
439 (Table 3).

440 Enrichment factors indicated a general accumulation of organic matter in the SML with respect to
441 the ULW (Figure 6), which happened at most stations. Thereby, clear differences were observed
442 between EF values of different components. The highest enrichment was observed for FAA that
443 were enriched more than 10-fold at some stations. Moreover, FAA were consistently enriched in
444 the SML, except for one station where the lowest FAA concentration was determined (49 nmol L^{-1}).
445 The largest variability of EF was observed for abundance and total area of gel particles. For
446 TEP total area, values of EF ranged between 0.2-12, with highest EF observed at the coastal
447 upwelling station 14_1, where the wind speed recorded was 0.6 m s^{-1} . In proximity of this station,
448 the lowest EF of TEP was determined (station 15_3) indicating a clear depletion at wind speed of
449 7 m s^{-1} . The EF of CSP total area ranged between 0.4 and 4.8. Thus highest EF of CSP was
450 clearly lower than for TEP, and in contrast to TEP it was observed at the more offshore station
451 18_2 at a higher wind speed rate of 9.2 m s^{-1} . Total and dissolved hydrolysable amino acids
452 (THAA, DHAA) were enriched in the SML at almost all stations (Figure 6), with EF in the range

453 0.8 - 4.6 (DHAA) and 0.4 - 3.4 (THAA). Median EFs were 1.7 and 1.4 for DHAA and THAA,
454 respectively.

455 Concentration of TCCHO, DCCHO in the SML were often similar to the ULW, with EF values
456 ranging between 0.6 and 1.4 (DCCHO) and between 0.3 and 1.7 (TCCHO), respectively.

457 In general, variability of EF was smaller for dissolved than for particulate organic compounds,
458 suggesting differences in the accumulation dynamics.

459 In contrast to all organic, chemical compounds, bacteria were found to be depleted in the SML at
460 almost all stations (Figure 6), having a median EF of 0.8

461

462 **3.4. Size distribution of gel particles within the SML**

463 Abundance of gel particles in the SML and ULW decreased with increasing particle size
464 according to the power law function given in eq. 2 (Figure 8). The parameter δ describes the
465 slope of the particles size spectrum. Lower values of δ indicate relatively higher abundance of
466 smaller particles. Data fits to the function were very well described for each sample with $r^2 > 0.90$,
467 yielding a standard error for δ of $< 20\%$. For TEP, δ varied between -2.63 and -1.38 (mean
468 value: -1.86, SD: 0.27, $n=39$) for particles in the SML and between -2.25 and -1.25 (mean value:
469 -1.70, SD: 0.30, $n=39$) for particles in the ULW. To compare the size distribution of TEP in the
470 SML and the ULW, we calculated the slope ratio ($\delta^* = \delta_{SML} / \delta_{ULW}$) (Figure 9). Size distributions of
471 TEP in the SML and ULW were generally quite similar yielding δ^*_{TEP} in the range of 0.78-1.42,
472 with a median value of 1.1. Nevertheless, spatial differences were observed, with $\delta^*_{TEP} < 0.95$ at
473 the more coastal northern stations and $\delta^*_{TEP} > 1.1$ more offshore at the southern stations (Figure
474 9). At the upwelling stations with high TEP abundance slopes of SML and ULW were very
475 similar, yielding δ^*_{TEP} in the range 0.95 - 1.1. This showed a relatively higher abundance of
476 smaller TEP in the SML at the offshore stations, whereas relatively more, larger sized TEP were

477 present close to the coast in the northern part of the study region. This comparison also showed
478 that sampling of TEP from the SML with a glass plate does not bias TEP size distribution, e.g. by
479 inducing particle aggregation during sampling. Such a bias would be expected especially at
480 stations where TEP was highly abundant, like at the upwelling stations. However, particularly at
481 those stations no difference in size distributions of TEP in the SML and ULW was observed.
482 Fractal scaling exponents of TEP were estimated from eq. 3 and yielded $D=2.51$ for both SML
483 and ULW samples ($D_{\text{SML}}=2.51\pm 0.015$ $n=39$; $D_{\text{ULW}}=2.51\pm 0.011$). The very similar fractal
484 dimension for TEP in the SML and ULW suggests that TEP in the SML and in the bulk water are
485 formed by similar aggregation processes. The value of $D=2.51$ estimated in this study is close to
486 2.55 proposed by Mari and Burd (1998) for seawater TEP.

487 In the SML, the number of TEP in the smallest size class (1.25-1.77 μm) ranged from 96 to
488 1.38×10^4 mL^{-1} , and included on average $61\pm 5.2\%$ of all TEP. For CSP, variability of abundance
489 in the 1.25-1.77 μm size class was much smaller and ranged between 1.46×10^4 and 2.33×10^5 mL^{-1} .
490 Although CSP thus represented the largest fraction of small gel particles, the relative
491 abundance of CSP in the smallest size fraction was lower, yielding an average contribution of
492 $52\pm 6.0\%$ of all CSP. Similar to TEP, size distribution of CSP followed the power law
493 relationship of eq. 2, yielding δ values between -1.12 and -2.01 (mean value: -1.44, SD: 0.20) for
494 particles in the SML and between -1.11 and -1.88 (mean value: -1.39, SD: 0.17) for particles in
495 the ULW. With $D=2.50\pm 0.008$, the fractal dimension of CSP was almost identical to that of TEP,
496 suggesting that similar processes, i.e. shear induced aggregation, are responsible for CSP
497 formation. The slope ratio, δ^* , for CSP varied between 0.77 and 1.32, with a median value of 1.0.
498 No spatial pattern was observed for the distribution of δ^*_{CSP} . Slopes of the size distribution of
499 CSP in the SML and ULW were not significantly different ($p=0.176$, $n=32$, paired t -test),

500 indicating that CSP size distribution, similarly to TEP, is not biased by the sampling approach of
501 the glass plate.

502 No overall relationship was established between the slope of the size distribution of TEP and
503 wind velocity (δ_{TEP} vs. wind speed: $r=-0.19$, $n=39$, $p=0.20$). However, TEP size distribution was
504 much steeper at the station with highest wind speed compared to the one with lowest wind
505 velocity (δ_{TEP} at $0.6 \text{ m s}^{-1} = -1.51$, $r^2=0.95$, $n=7$; δ_{TEP} at $9.0 \text{ m s}^{-1} = -2.31$, $r^2=0.95$, $n=7$) (Figure
506 8a). In particular, at the high wind speed a loss of larger TEP, i.e. $>7 \mu\text{m}$ was observed in the
507 SML compared to the ULW and relative to the low wind speed station.

508 For CSP a significant inverse relationship was observed between the slope δ and wind speed
509 (δ_{CSP} vs. wind speed: $r=-0.61$, $n=37$, $p<0.001$). A loss of larger CSP was also observed by direct
510 comparison between low and high wind speed stations (δ_{CSP} at $0.6 \text{ m s}^{-1} = -1.12$, $r^2=0.92$, $n=7$;
511 δ_{TEP} at $9.0 \text{ m s}^{-1} = -1.45$, $r^2=0.97$, $n=7$) (Figure 8b).

512

513 **4. Discussion**

514 It has been suggested that the presence of organic matter in the SML influences a series of
515 processes relevant to air-sea exchange of gases, dissolved and particulate components. EBU'S are
516 characterized by high biological productivity and strong across shelf gradients of organic matter
517 concentration (Capone and Hutchins, 2013). Therefore EBU'S are ideal model systems to study
518 the linkages of biological productivity and SML properties, with respect to characteristics of
519 organic matter composition and factors controlling organic matter enrichment in the SML.

520

521 **4.1. Organic matter characteristics of the SML in the upwelling region off Peru**

522 Strong horizontal gradients in organic matter concentration of the SML were observed for the
523 coastal and shelf-break region off Peru with generally higher organic matter concentrations in the

524 SML towards the area of upwelling of colder, nutrient-rich deep water. Hence, increasing
525 ecosystem productivity is one likely factor responsible for higher concentrations of organic
526 components in the SML. Significant correlations between organic matter concentration in the
527 SML and in the ULW were determined and showed that the SML basically reflects the
528 underlying seawater system. The close connectivity between SML organic properties and
529 biological development was also shown during a recent mesocosm study, indicating that
530 ecosystem changes impact SML organic matter composition and concentration (Galvani et al.,
531 2014). Despite this finding that relates to a more general characteristic of the SML, clear
532 differences in the accumulation behavior of different organic matter components were determined
533 during this study and are in good accordance with previous observations. A generally higher
534 SML accumulation was observed for amino acids compared to carbohydrates. Significant
535 enrichment of amino acids in the SML has been determined previously for coastal as well as open
536 ocean sites, and higher accumulation of FAA compared to DHAA and THAA, as also observed
537 during this study, appears to be a consistent SML feature (Carlucci et al., 1992; Henrichs and
538 Williams, 1985; Kuznetsova and Lee, 2002, 2001; Kuznetsova et al., 2004; Reinthaler et al.,
539 2008). As for this study, wind velocity and temperature have not been identified as physical
540 factors responsible for amino acid enrichment in the past (Kuznetsova et al., 2004). FAA and
541 DHAA are labile to semi-labile substrates and taken-up by heterotrophic microorganisms (Keil
542 and Kirchman, 1992). Turnover times of these components in the water column are usually in the
543 range of minutes to days (Benner, 2002; Fuhrman and Ferguson, 1986). The observed
544 accumulation of FAA and DHAA in the SML may therefore be related to a reduced activity of
545 bacteria. For different coastal Baltic Sea sites, Stolle et al. (2009) determined a lowered bacterial
546 biomass production in the SML, despite bacterial cell numbers being similar to those in the
547 ULW. During M91 bacteria were mostly depleted in the SML compared to the ULW supporting

548 the idea of the SML being an ‘extreme environment’ for bacteria. Earlier studies showed that
549 some bacteria may be adapted to UV radiation in the SML as well as in the ULW (Agogué et al.,
550 2005; Carlucci et al., 1985). Amino acid consumption by bacterioneuston under UV-B stress may
551 be reduced (Santos et al., 2012), which may give an explanation for the higher concentrations of
552 FAA and DHAA in the SML during M91. However, no significant correlation between bacterial
553 abundance and UV radiation or between UV radiation and amino acid concentrations in the
554 different pools was observed during this study, suggesting that at most stations history rather than
555 instantaneous UV radiation is if at all responsible for controlling bacteria and organic matter
556 components in the SML.

557 SML thickness during this study was significantly related to TOC concentration, but not to wind
558 speed. A thickening of the SML with increasing wind speed up to 8 m s^{-1} has been observed by
559 Falkowska (1999) from samples collected in the Baltic Sea and explained by increased advective
560 transport of organic matter to the SML, e.g. through bubble adsorption, at higher turbulence.
561 During M91, accumulation of organic matter in the SML was higher at the upwelling stations
562 where wind speed often was quite low. Hence, a higher source of organic matter in the ULW may
563 have counterbalanced the wind speed effect.

564
565 Wind speed, however, was determined as a factor controlling accumulation of particulate
566 material, in particular TEP, in the SML in addition to the dynamics occurring in the ULW. TEP
567 are marine gel particles hypothesized to be neutrally or positively buoyant thanks to their high
568 water content (Azetsu-Scott and Passow, 2004; Engel and Schartau, 1999). TEP were moreover
569 suggested to form within the SML, either by wind-shear induced aggregation of precursors or due
570 to coalescence of pre-cursor molecules, primarily polysaccharides, when entrained air bubbles
571 burst at the sea surface (Wurl et al., 2011). Adsorption of DOM onto bubble surfaces and TEP

572 formation by bubble bursting have been determined during experimental flotation and bubbling
573 studies using surface seawater from different locations (Wallace and Duce, 1978; Zhou et al.,
574 1998). Bubble scavenging of DOM in the upper water column may thus be responsible for high
575 concentrations of TEP at the SML, because more TEP precursors are lifted up the water-column
576 (Gao et al., 2012; Wurl et al., 2011). In addition, compression and dilatation of the SML due to
577 capillary waves may increase the rate of polymer collision, subsequently facilitating gel
578 aggregation (Carlson, 1993). During M91, TEP enrichment in the SML was inversely related to
579 wind speed, supporting earlier observations of Wurl and colleagues (Wurl et al., 2009; Wurl et
580 al., 2011). However, in contrast to earlier observations showing EF values >1 for TEP in the
581 SML also at higher wind speed, we found the SML to be depleted of TEP at wind speed of ~ 5 m
582 s^{-1} and above. It has been suggested that TEP aggregation rates in the SML are higher than in the
583 ULW, due to enhance collision rates by shear or bubble bursting. TEP have been shown to
584 control coagulation efficiencies of solid particles, such as diatoms and coccolithophores (Chow et
585 al., 2015; Engel, 2000; Logan et al., 1995). At higher wind speed, increased aggregation rates of
586 TEP with solid particles, eventually containing mineral ballast, may thus favor the formation of
587 aggregates that become negatively buoyant and sink out of the SML. This, may explain the
588 observed loss of larger TEP ($>7 \mu m$) from the SML relative to the ULW and to the SML at low
589 wind speed. Enhanced aggregation rates could then also explain the inverse relationship between
590 POC and wind speed, observed during this study.

591
592 In contrast to TEP, no impact of wind speed was determined for CSP accumulation, or for CSP
593 enrichment in the SML. Moreover, clear spatial differences were observed for the distribution of
594 TEP and CSP in the SML. Although both TEP and CSP are gel particles that form from dissolved
595 organic precursors released by microorganisms, their spatial and temporal occurrence in marine

596 systems can be quite different, e.g. TEP accumulate towards the end of phytoplankton blooms
597 while CSP rather co-occur with maximum phytoplankton abundance (Cisternas-Novoa et al.,
598 2015; Engel et al., 2015). Moreover, the depth distribution of TEP and CSP was shown to be
599 different for open ocean sites (Cisternas-Novoa et al., 2015). These spatial and temporal
600 differences in the occurrence of TEP and CSP in the water column may explain the spatial
601 separation of both types of marine gels in the SML observed during this study. However, the
602 observed differences in relation to wind speed suggest that additional factors control the
603 enrichment of TEP and CSP in the SML. It has been shown that CSP are less prone to
604 aggregation than TEP (Engel et al., 2015; Prieto et al., 2002). Similarly, CSP may be less
605 involved in aggregation formation and sinking out of the SML at higher wind speed. Yet,
606 similarly to TEP, larger CSP were observed in the SML at low wind speed suggesting that both
607 kind of gels may be involved in slick formation that becomes disrupted when wind speed
608 increases.

609

610

611 **4.2. Implications of organic matter accumulation in EBUS**

612 **4.2.1. Air-Sea gas exchange**

613 Although the SML and surface active substances (surfactants) within are widely believed
614 affecting the exchange of gases and heat at the air-sea interface (Davies, 1966; Frew, 1997; Salter
615 et al., 2011), particularly at lower wind speed (Liss, 1983), we still have little quantitative
616 knowledge on how natural organic components at the immediate sea-surface alter the gas transfer
617 velocity in water (kw). Our data showed a depletion of the SML with respect to TEP and POC at
618 wind speeds $>5 \text{ m s}^{-1}$, suggesting that an effect of these ‘insoluble’ components on gas exchange
619 is, if any, operating only at low wind speed. Due to their fractal scaling, gel particles have a

620 relatively large surface to volume ratio and may act as a cover, reducing molecular diffusion rates
621 at the interface between air and sea.

622 Accumulation of dissolved organic components in the SML during M91 was not related to wind
623 speed. DCCHO and DHAA concentration representing fresh DOM were highest at the upwelling
624 sites and therefore negatively related to seawater temperature. DOM, such as DCCHO and
625 chromophoric dissolved organic matter (CDOM), have demonstrated surfactant properties and
626 reduced gas transfer velocity in water (kw) at low wind speed in laboratory and field experiments
627 (Frew et al., 2004; Frew et al., 1990). The reduction of kw is thereby believed to be related to a
628 dampening of small, capillary waves. Salter et al. (2011) recently showed that artificial
629 surfactants can suppress gas transfer velocity by up to 55% at sea. Suppression of k_{666} (i.e. kw
630 normalized to a Schmidt number of 666) during their field study was depending on wind speed,
631 but was detected up to 11 m s^{-1} , encompassing the full range of wind speed determined during
632 M91. Thus, accumulation of natural DOM particularly in upwelling regimes with high biological
633 production and coastal wind shelter as observed during this study may have an influence on gas
634 exchanges rates as well.

635
636 Across the SML, the diffusivity of climate relevant gases such as methane (CH_4), has been
637 proposed being mediated by SML bacteria, as possible sink (Upstill-Goddard et al., 2003) or
638 source of this compound (Cunliffe et al., 2013). About ~ 30 % of the atmospheric concentration
639 of nitrous oxide (N_2O), one of the strongest greenhouse gases and responsible for ozone
640 depletion, is supported by oceanic sources (Solomon et al., 2007). Of total oceanic N_2O
641 production, oxygen minimum zones (OMZs) contribute about 25-75 % (Bange et al., 2001). In
642 EBU'S, high primary production and induced high aerobic remineralization associated with
643 large-scale circulation maintain the presence of OMZs (Gutknecht et al., 2013; Paulmier and

644 Ruiz-Pino, 2009), which, in the last decades, have been expanding and intensifying due to
645 enhanced stratification and reduced ventilation (Keeling et al., 2010; Stramma et al., 2008).
646 During M91, N₂O concentration in surface waters was highly supersaturated at the upwelling
647 sites and in particular at station 14_1 (Arevalo-Martinez et al., 2015). Although a direct influence
648 of organic matter in the SML on gas-exchange was not investigated during M91, it can be
649 assumed that the high enrichment of organic components in the SML observed the upwelling
650 sites was one factor contributing to N₂O supersaturation.

651 Our study was intended to understand how organic matter accumulates in the SML, which might
652 mediate the transfer rate of trace- and greenhouse gases such as N₂O in oceanic regions like
653 OMZ's affected by a changing climate. A recent laboratory study reported π non-covalent
654 interactions of N₂O with phenols, suggesting a possible important role of N₂O in biological
655 processes by specifically binding to phenolic groups as those of the amino acids tyrosine and
656 phenylalanine (Cao et al., 2014). Tyrosine and phenylalanine in the SML of our study represented
657 a small molar percentage of total amino acids pool (data not shown), but were present. As we
658 found evidence of overall amino acids SML accumulation during our cruise, for those amino
659 acids in particular the median EF both in the total (THAA) and in the dissolved (DHAA) fraction
660 was > 1 , suggesting a possible interaction of specific SML organics with N₂O in the coastal
661 upwelling region off Peru. Although the experiment conducted by Cao and colleagues cannot be
662 directly translated to our setting, it provides interesting ideas for the interaction of N₂O with
663 biological macromolecules worth further investigation.

664 Overall, our results showed that accumulation of organic substances occurs in EBU's and is
665 related to the increased biological production. Hence, the organic SML may play a particularly
666 important role for exchange of climate relevant gases that are associated to high organic matter
667 production and resulting anoxia in upwelling systems like the one off Peru.

668 **4.2.2. Organic aerosol production**

669 The structure of sea-spray aerosols (SSA) originating by bubble bursting at the sea surface is a
670 function of biological, chemical and physical properties of the SML, which may comprise a vast
671 array of organic surface-active compounds, microorganisms, and exopolymer gels (Leck and
672 Bigg, 2005; Quinn and Bates, 2011; Wilson et al., 2015). Despite recent evidences showing that
673 high levels of chlorophyll-*a* are not directly related to the organic carbon content of SSA (Quinn
674 et al., 2014), still organic SSA largely derive from the oceanic surface layer and therefore are also
675 subject to the effects of climate change on marine systems (Andreae and Crutzen, 1997).
676 Polysaccharides and polysaccharidic nanogels (Orellana et al., 2011; Russell et al., 2010) as well
677 as particulate amino acids and proteinaceous compounds (Kuznetsova et al., 2005) are present in
678 organic SSA particles. During M91, we found a different accumulation behavior of TEP and CSP
679 in the SML. TEP showed a close inverse relationship to wind speed, being depleted in the SML
680 above 5 m s^{-1} , while particulate proteinaceous compounds (CSP) accumulated independently of
681 wind speed. Submicron gels embedded in sea spray may represent an important source for
682 primary organic aerosols in the more offshore wind exposed regions. TEP as well as dissolved
683 polysaccharides include sugars with carboxylic groups such as uronic acids and may contribute to
684 the relatively high fraction of carboxylic acid that was observed in the organic matter component
685 of marine aerosols (Hawkins et al., 2010). In the upwelling region off Peru the wind-driven
686 export of polysaccharidic components to the atmosphere thus might represent a loss-pathway of
687 these organic compounds from the SML that would then contribute to a larger extent to the
688 organic SSA mass. Proteinaceous compounds, including CSP, are probably more stable at the sea
689 surface and may contribute to organic mass in aerosols even at higher wind speed.

690 However, future studies that investigate gel particles within the SML and in SSA are needed to
691 clarify if the observed loss of TEP from the SML at higher wind speeds is indeed related to a
692 transport of TEP to the atmosphere, or if CSP contribute to organic aerosol mass.

693 The accumulation of organic matter in the SML, and the distinct behavior of certain compounds
694 at the water-air interface is certainly an important issue for all exchange processes between the
695 ocean and the atmosphere that needs to be further exploited.

696

697

698 **Acknowledgements**

699

700 We thank the captain and crew of *R/V METEOR* during cruise leg M91 for logistic support
701 during sampling, especially help related to the rubber boat operation, as well as H. Bange as chief
702 scientist and all the scientific crew. A great acknowledgement goes to J. Roa for helping with
703 SML sampling on board and for TOC/TN and carbohydrates analysis, respectively. Further
704 technical help was provided by R. Flerus, S.Manandhar and N. Bijma for amino acids and
705 microscopy analysis, as well as T. Klüver for flow-cytometry counts. This work was supported
706 by BMBF project SOPRAN II and III (Surface Ocean Processes in the Anthropocene, 03F0611C-
707 TP01 and 03F0662A-TP2.2).

708

709 **References:**

- 710
- 711 Agogu , H., Casamayor, E. O., Bourrain, M., Obernosterer, I., Joux, F., Herndl, G. J., and Lebaron,
712 P.: A survey on bacteria inhabiting the sea surface microlayer of coastal ecosystems, *FEMS*
713 *Microbiology Ecology*, 54, 269-280, 2005.
- 714 Andreae, M. O. and Crutzen, P. J.: Atmospheric Aerosols: Biogeochemical Sources and Role in
715 Atmospheric Chemistry, *Science*, 276, 1052-1058, 1997.
- 716 Arevalo-Martinez, D. L., Kock, A., Loscher, C. R., Schmitz, R. A., and Bange, H. W.: Massive
717 nitrous oxide emissions from the tropical South Pacific Ocean, *Nature Geosci*, 8, 530-533, 2015.
- 718 Azetsu-Scott, K. and Passow, U.: Ascending marine particles: significance of transparent
719 exopolymer particles (TEP) in the upper ocean. , *Limnol. Oceanogr.*, 49, 741-748, 2004.
- 720 Bange, H. W.: Surface Ocean - Lower Atmosphere Study (SOLAS) in the upwelling region off Peru
721 - Cruise No. M91 – December 01 – December 26, 2012 – Callao (Peru) – Callao (Peru), Bremen,
722 69 pp., 2013.
- 723 Bange, H. W., Rapsomanikis, S., and Andreae, M. O.: Nitrous oxide cycling in the Arabian Sea, *J.*
724 *Geophys. Res-Oceans*, 106, 1053-1065, 2001.
- 725 Bar-Zeev, E., Berman-Frank, I., Girshevitz, O., and Berman, T.: Revised paradigm of aquatic
726 biofilm formation facilitated by microgel transparent exopolymer particles, *Proceedings of the*
727 *National Academy of Sciences*, 109, 9119-9124, 2012.
- 728 Benner, R.: Chemical composition and reactivity. In: *Biogeochemistry of marine dissolved*
729 *organic matter*, Hansell, D. A. and Carlson, D. J. (Eds.), Academic Press - Elsevier, 2002.
- 730 Bigg, K. E., Leck, C., and Tranvik, L.: Particulates of the surface microlayer of open water in the
731 central Arctic Ocean in summer, *Mar. Chem.*, 91, 131-141, 2004.
- 732 Cao, Q., Gor, G. Y., Krogh-Jespersen, K., and Khriachtchev, L.: Non-covalent interactions of
733 nitrous oxide with aromatic compounds: Spectroscopic and computational evidence for the
734 formation of 1:1 complexes, *J. Chem. Phys.*, 140, 144304, 2014.
- 735 Capone, D. G. and Hutchins, D. A.: Microbial biogeochemistry of coastal upwelling regimes in a
736 changing ocean, *Nat. Geosci.*, 6, 711-717, 2013.
- 737 Carlson, D.: The Early Diagenesis of Organic Matter: Reaction at the Air-Sea Interface. In:
738 *Organic Geochemistry*, Engel, M. and Macko, S. (Eds.), Topics in Geobiology, Springer US, 1993.
- 739 Carlson, D. J.: A field evaluation of plate and screen microlayer sampling techniques, *Mar.*
740 *Chem.*, 11, 189-208, 1982.
- 741 Carlucci, A. F., Craven, D. B., and Henrichs, S. M.: Surface-film microheterotrophs: amino acid
742 metabolism and solar radiation effects on their activities, *Marine Biology*, 85, 13-22, 1985.
- 743 Carlucci, A. F., Wolgast, D. M., and Craven, D. B.: Microbial Populations in Surface Films: Amino
744 Acid Dynamics in Nearshore and Offshore Waters off Southern California, *J. geophys. Res.*, 97,
745 5271-5280, 1992.
- 746 Carr, M.-E. and Kearns, E. J.: Production regimes in four Eastern Boundary Current systems,
747 *Deep Sea Research Part II: Topical Studies in Oceanography*, 50, 3199-3221, 2003.
- 748 Chin, W.-C., Orellana, M. V., and Verdugo, P.: Spontaneous assembly of marine dissolved
749 organic matter into polymer gels, *Nature*, 391, 568-572, 1998.
- 750 Chow, J. S., Lee, C., and Engel, A.: The influence of extracellular polysaccharides, growth rate,
751 and free coccoliths on the coagulation efficiency of *Emiliania huxleyi*, *Marine Chemistry*, doi:
752 <http://dx.doi.org/10.1016/j.marchem.2015.04.010>, 2015. 2015.

- 753 Cisternas-Nova, C., Lee, C., and Engel, A.: Transparent exopolymer particles (TEP) and
754 Coomassie stainable particles (CSP): Differences between their origin and vertical distributions
755 in the ocean, *Marine Chemistry*, doi: <http://dx.doi.org/10.1016/j.marchem.2015.03.009>, 2015.
756 2015.
- 757 Cunliffe, M., Engel, A., Frka, S., Gašparović, B., Guitart, C., Murrell, J. C., Salter, M., Stolle, C.,
758 Upstill-Goddard, R., and Wurl, O.: Sea surface microlayers: A unified physicochemical and
759 biological perspective of the air-ocean interface, *Progr. Oceanogr.*, 109, 104-116, 2013.
- 760 Cunliffe, M. and Murrell, J. C.: The sea-surface microlayer is a gelatinous biofilm, *The ISME*
761 *journal*, 3, 1001-1003, 2009.
- 762 Cunliffe, M., Upstill-Goddard, R. C., and Murrell, J. C.: Microbiology of aquatic surface
763 microlayers, *FEMS Microbiol. Rev.*, 35, 233-246, 2011.
- 764 Cunliffe, M. and Wurl, O.: Guide to best practices to study the ocean's surface., Plymouth, UK,
765 2014.
- 766 Davies, J. T.: The Effects of Surface Films in Damping Eddies at a Free Surface of a Turbulent
767 Liquid, 1966.
- 768 Dickson, A. G., Sabine, C. L., and Christian, J. R.: Guide to best practices for ocean CO₂
769 measurements, PICES, 2007.
- 770 Dittmar, T., Cherrier, J., and Ludwiczowski, K.-U.: The Analysis of Amino Acids in Seawater. In:
771 Practical Guidelines for the Analysis of Seawater, CRC Press, 2009.
- 772 Engel, A.: Determination of Marine Gel Particles. In: Practical Guidelines for the Analysis of
773 Seawater, CRC Press, 2009.
- 774 Engel, A.: The role of transparent exopolymer particles (TEP) in the increase in apparent particle
775 stickiness (α) during the decline of a diatom bloom, *Journal of Plankton Research*, 22, 485-497,
776 2000.
- 777 Engel, A., Borchard, C., Loginova, A., Meyer, J., Hauss, H., and Kiko, R.: Effects of varied nitrate
778 and phosphate supply on polysaccharidic and proteinaceous gel particles production during
779 tropical phytoplankton bloom experiments, *Biogeosciences Discuss.*, 12, 6589-6635, 2015.
- 780 Engel, A., Borchard, C., Piontek, J., Schulz, K. G., Riebesell, U., and Bellerby, R.: CO₂ increases
781 14C primary production in an Arctic plankton community, *Biogeosciences*, 10, 1291-1308, 2013.
- 782 Engel, A. and Händel, N.: A novel protocol for determining the concentration and composition of
783 sugars in particulate and in high molecular weight dissolved organic matter (HMW-DOM) in
784 seawater, *Marine Chemistry*, 127, 180-191, 2011.
- 785 Engel, A. and Schartau, M.: Influence of transparent exopolymer particles (TEP) on sinking
786 velocity of *Nitzschia closterium* aggregates, *Marine Ecology Progress Series*, 182, 69-76, 1999.
- 787 Engel, A., Thoms, S., Riebesell, U., Rochelle-Newall, E., and Zondervan, I.: Polysaccharide
788 aggregation as a potential sink of marine dissolved organic carbon, *Nature*, 428, 929-932, 2004.
- 789 Falkowska, L.: Sea surface microlayer: a field evaluation of teflon plate, glass plate and screen
790 sampling techniques. Part 1. Thickness of microlayer samples and relation to wind speed,
791 *Oceanologia*, 41, 211-221, 1999.
- 792 Frew, N. M.: The role of organic films in air-sea gas exchange. In: *The Sea Surface and Global*
793 *Change*, Liss, P. S. and Duce, R. A. (Eds.), Cambridge University Press, UK, 1997.
- 794 Frew, N. M., Bock, E. J., Schimpf, U., Hara, T., Haußecker, H., Edson, J. B., McGillis, W. R., Nelson,
795 R. K., McKenna, S. P., Uz, B. M., and Jähne, B.: Air-sea gas transfer: Its dependence on wind
796 stress, small-scale roughness, and surface films, *Journal of Geophysical Research: Oceans*, 109,
797 n/a-n/a, 2004.

- 798 Frew, N. M., Goldman, J. C., Dennett, M. R., and Johnson, A. S.: Impact of phytoplankton-
799 generated surfactants on air-sea gas exchange, *Journal of Geophysical Research: Oceans*, 95,
800 3337-3352, 1990.
- 801 Fuhrman, J. A. and Ferguson, R. L.: Nanomolar concentrations and rapid turnover of dissolved
802 free amino acids in seawater: agreement between chemical and microbiological measurements,
803 *Marine Ecology Progress Series*, 33, 237-242, 1986.
- 804 Galgani, L. and Engel, A.: Accumulation of Gel Particles in the Sea-Surface Microlayer during an
805 Experimental Study with the Diatom *Thalassiosira weissflogii*, *International Journal of*
806 *Geosciences*, 4, 129-145, 2013.
- 807 Galgani, L., Stolle, C., Endres, S., Schulz, K. G., and Engel, A.: Effects of ocean acidification on the
808 biogenic composition of the sea-surface microlayer: Results from a mesocosm study, *J.*
809 *Geophys. Res-Oceans*, 119, 7911-7924, 2014.
- 810 Gao, Q., Leck, C., Rauschenberg, C., and Matrai, P. A.: On the chemical dynamics of extracellular
811 polysaccharides in the high Arctic surface microlayer, *Ocean Sci.*, 8, 401-418, 2012.
- 812 Garreaud, R. D., Rutllant, J. A., Muñoz, R. C., Rahn, D. A., Ramos, M., and Figueroa, D.: VOCALS-
813 CUpEx: the Chilean Upwelling Experiment, *Atmos. Chem. Phys.*, 11, 2015-2029, 2011.
- 814 GESAMP: The Sea-Surface Microlayer and its Role in Global Change. Reports and Studies, WMO,
815 1995.
- 816 Gutknecht, E., Dadou, I., Marchesiello, P., Cambon, G., Le Vu, B., Sudre, J., Garçon, V., Machu, E.,
817 Rixen, T., Kock, A., Flohr, A., Paulmier, A., and Lavik, G.: Nitrogen transfers off Walvis Bay: a 3-D
818 coupled physical/biogeochemical modeling approach in the Namibian upwelling system,
819 *Biogeosciences*, 10, 4117-4135, 2013.
- 820 Harvey, G. W. and Burzell, L. A.: A simple microlayer method for small samples, *Limnol.*
821 *Oceanogr.*, 11, 608-614, 1972.
- 822 Hatcher, R. F. and Parker, B. C.: Laboratory comparisons of four surface microlayer samplers¹,
823 *Limnology and Oceanography*, 19, 162-165, 1974.
- 824 Hawkins, L. N., Russell, L. M., Covert, D. S., Quinn, P. K., and Bates, T. S.: Carboxylic acids,
825 sulfates, and organosulfates in processed continental organic aerosol over the southeast Pacific
826 Ocean during VOCALS-REx 2008, *Journal of Geophysical Research: Atmospheres*, 115, n/a-n/a,
827 2010.
- 828 Henrichs, S. M. and Williams, P. M.: Dissolved and particulate amino acids and carbohydrates in
829 the sea surface microlayer, *Marine Chemistry*, 17, 141-163, 1985.
- 830 Hu, H., Bourbonnais, A., Larkum, J., Bange, H. W., and Altabet, M. A.: Nitrogen cycling in shallow
831 low oxygen coastal waters off Peru from nitrite and nitrate nitrogen and oxygen isotopes,
832 *Biogeosciences Discuss.*, 12, 7257-7299, 2015.
- 833 Jähne, B. and Haußecker, H.: AIR-WATER GAS EXCHANGE, *Annual Review of Fluid Mechanics*, 30,
834 443-468, 1998.
- 835 Keeling, R. F., Körtzinger, A., and Gruber, N.: Ocean Deoxygenation in a Warming World, *Annu.*
836 *Rev. Mar. Sci.*, 2, 199-229, 2010.
- 837 Keil, R. G. and Kirchman, D. L.: Bacterial Hydrolysis of Protein and Methylated Protein and Its
838 Implications for Studies of Protein Degradation in Aquatic Systems, *Applied and Environmental*
839 *Microbiology*, 58, 1374-1375, 1992.
- 840 Kuznetsova, M. and Lee, C.: Dissolved free and combined amino acids in nearshore seawater,
841 sea surface microlayers and foams: Influence of extracellular hydrolysis, *Aquatic Sciences -*
842 *Research Across Boundaries*, 64, 252-268, 2002.

- 843 Kuznetsova, M. and Lee, C.: Enhanced extracellular enzymatic peptide hydrolysis in the sea-
844 surface microlayer, *Marine Chemistry*, 73, 319-332, 2001.
- 845 Kuznetsova, M., Lee, C., and Aller, J.: Characterization of the proteinaceous matter in marine
846 aerosols, *Marine Chemistry*, 96, 359-377, 2005.
- 847 Kuznetsova, M., Lee, C., and Aller, J.: Enrichment of amino acids in the sea surface microlayer at
848 coastal and open ocean sites in the North Atlantic Ocean, *Limnol. Oceanogr.*, 49, 1605-1619,
849 2004.
- 850 Lachkar, Z. and Gruber, N.: What controls biological production in coastal upwelling systems?
851 Insights from a comparative modeling study, *Biogeosciences*, 8, 2961-2976, 2011.
- 852 Laß, K., Bange, H. W., and Friedrichs, G.: Seasonal signatures in SFG vibrational spectra of the
853 sea surface nanolayer at Boknis Eck Time Series Station (SW Baltic Sea), *Biogeosciences*, 10,
854 5325-5334, 2013.
- 855 Leck, C. and Bigg, E. K.: Source and evolution of the marine aerosol—A new perspective,
856 *Geophysical Research Letters*, 32, L19803, 2005.
- 857 Lindroth, P. and Mopper, K.: High performance liquid chromatographic determination of
858 subpicomole amounts of amino acids by precolumn fluorescence derivatization with o-
859 phthaldialdehyde, *Anal. Chem.*, 51, 1667-1674, 1979.
- 860 Liss, P. S.: Gas Transfer: Experiments and Geochemical Implications. In: *Air-Sea Exchange of*
861 *Gases and Particles*, Liss, P. and Slinn, W. G. (Eds.), NATO ASI Series, Springer Netherlands, 1983.
- 862 Liss, P. S. and Duce, R. A.: *The Sea Surface and Global Change*, Cambridge University Press, 2005.
- 863 Logan, B. E., Passow, U., Alldredge, A. L., Grossartt, H.-P., and Simont, M.: Rapid formation and
864 sedimentation of large aggregates is predictable from coagulation rates (half-lives) of
865 transparent exopolymer particles (TEP), *Deep Sea Research Part II: Topical Studies in*
866 *Oceanography*, 42, 203-214, 1995.
- 867 Long, R. A. and Azam, F.: Abundant protein-containing particles in the sea, *Aquatic Microbial*
868 *Ecology*, 10, 213-221, 1996.
- 869 Mari, X. and Burd, A.: Seasonal size spectra of transparent exopolymeric particles (TEP) in a
870 coastal sea and comparison with those predicted using coagulation theory, *Marine Ecology*
871 *Progress Series*, 163, 63-76, 1998.
- 872 Mari, X. and Kiørboe, T.: Abundance, size distribution and bacterial colonization of transparent
873 exopolymeric particles (TEP) during spring in the Kattegat, *Journal of Plankton Research*, 18,
874 969-986, 1996.
- 875 Matrai, P. A., Tranvik, L., Leck, C., and Knulst, J. C.: Are high Arctic surface microlayers a
876 potential source of aerosol organic precursors?, *Mar. Chem.*, 108, 109-122, 2008.
- 877 Meakin, P.: Fractal aggregates in geophysics, *Reviews of Geophysics*, 29, 317-354, 1991.
- 878 O'Dowd, C. D., Facchini, M. C., Cavalli, F., Ceburnis, D., Mircea, M., Decesari, S., Fuzzi, S., Yoon, Y.
879 J., and Putaud, J.-P.: Biogenically driven organic contribution to marine aerosol, *Nature*, 431,
880 676-680, 2004.
- 881 Orellana, M. V., Matrai, P. A., Leck, C., Rauschenberg, C. D., Lee, A. M., and Coz, E.: Marine
882 microgels as a source of cloud condensation nuclei in the high Arctic, *Proceedings of the*
883 *National Academy of Sciences*, 108, 13612-13617, 2011.
- 884 Panagiotopoulos, C., Sempéré, R., Lafont, R., and Kerhervé, P.: Sub-ambient temperature effects
885 on the separation of monosaccharides by high-performance anion-exchange chromatography
886 with pulse amperometric detection: Application to marine chemistry, *Journal of*
887 *Chromatography A*, 920, 13-22, 2001.

- 888 Passow, U.: Transparent exopolymer particles (TEP) in aquatic environments, *Progress in*
889 *Oceanography*, 55, 287-333, 2002.
- 890 Paulmier, A. and Ruiz-Pino, D.: Oxygen minimum zones (OMZs) in the modern ocean, *Progr.*
891 *Oceanogr.*, 80, 113-128, 2009.
- 892 Paulmier, A., Ruiz-Pino, D., and Garçon, V.: The oxygen minimum zone (OMZ) off Chile as
893 intense source of CO₂ and N₂O, *Cont. Shelf Res.*, 28, 2746-2756, 2008.
- 894 Paulmier, A., Ruiz-Pino, D., and Garçon, V.: CO₂ maximum in the oxygen minimum zone (OMZ),
895 *Biogeosciences*, 8, 239-252, 2011.
- 896 Prieto, L., Ruiz, J., Echevarría, F., García, C. M., Bartual, A., Gálvez, J. A., Corzo, A., and Macías,
897 D.: Scales and processes in the aggregation of diatom blooms: high time resolution and wide
898 size range records in a mesocosm study, *Deep Sea Research Part I: Oceanographic Research*
899 *Papers*, 49, 1233-1253, 2002.
- 900 Quinn, P. K. and Bates, T. S.: The case against climate regulation via oceanic phytoplankton
901 sulphur emissions, *Nature*, 480, 51-56, 2011.
- 902 Quinn, P. K., Bates, T. S., Schulz, K. S., Coffman, D. J., Frossard, A. A., Russell, L. M., Keene, W. C.,
903 and Kieber, D. J.: Contribution of sea surface carbon pool to organic matter enrichment in sea
904 spray aerosol, *Nature Geosci*, 7, 228-232, 2014.
- 905 Reinthaler, T., Sintes, E., and Herndl, G. J.: Dissolved organic matter and bacterial production
906 and respiration in the sea-surface microlayer of the open Atlantic and the western
907 Mediterranean Sea, *Limnol. Oceanogr.*, 53, 122-136, 2008.
- 908 Riebesell, U., Kortzinger, A., and Oschlies, A.: Tipping Elements in Earth Systems Special Feature:
909 Sensitivities of marine carbon fluxes to ocean change, *Proceedings of the National Academy of*
910 *Sciences*, 106, 20602-20609, 2009.
- 911 Russell, L. M., Hawkins, L. N., Frossard, A. A., Quinn, P. K., and Bates, T. S.: Carbohydrate-like
912 composition of submicron atmospheric particles and their production from ocean bubble
913 bursting, *Proceedings of the National Academy of Sciences*, 107, 6652-6657, 2010.
- 914 Salter, M. E., Upstill-Goddard, R. C., Nightingale, P. D., Archer, S. D., Blomquist, B., Ho, D. T.,
915 Huebert, B., Schlosser, P., and Yang, M.: Impact of an artificial surfactant release on air-sea gas
916 fluxes during Deep Ocean Gas Exchange Experiment II, *Journal of Geophysical Research: Oceans*,
917 116, C11016, 2011.
- 918 Santos, A. L., Oliveira, V., Baptista, I., Henriques, I., Gomes, N. C., Almeida, A., Correia, A., and
919 Cunha, A.: Effects of UV-B radiation on the structural and physiological diversity of
920 bacterioneuston and bacterioplankton, *Appl. Environ. Microbiol.*, 78, 2066-2069, 2012.
- 921 Schlitzer, R.: *Ocean Data View*. 2013.
- 922 Schulz, K. G., Bellerby, R. G. J., Brussaard, C. P. D., Büdenbender, J., Czerny, J., Engel, A., Fischer,
923 M., Koch-Klavnsen, S., Krug, S. A., Lischka, S., Ludwig, A., Meyerhøfer, M., Nondal, G., Silyakova,
924 A., Stühr, A., and Riebesell, U.: Temporal biomass dynamics of an Arctic plankton bloom in
925 response to increasing levels of atmospheric carbon dioxide, *Biogeosciences*, 10, 161-180, 2013.
- 926 Sieburth, J. M.: *Microbiological and organic-chemical processes in the surface and mixed layers -*
927 *Air-Sea exchange of Gases and Particles*, D.Reidel Publishing Company, 1983.
- 928 Solomon, S., Qin, D., Manning, M., Chen, Z., Marquis, M., Averyt, K. B., Tignor, M., and Miller, H.
929 L.: *Climate Change 2007: The Physical Science Basis. Contribution of Working Group I to the*
930 *Fourth Assessment Report of the Intergovernmental Panel on Climate Change*, Cambridge,
931 United Kingdom and New York, NY, USA, Cambridge University Press, 2007.

- 932 Steinfeldt, R., Sültenfuß, J., Dengler, M., Fischer, T., and Rhein, M.: Coastal upwelling off Peru
933 and Mauritania inferred from helium isotope disequilibrium, *Biogeosciences Discuss.*, 12, 11019-
934 11059, 2015.
- 935 Stolle, C., Nagel, K., Labrenz, M., and Jürgens, K.: Bacterial activity in the sea-surface microlayer:
936 in situ investigations in the Baltic Sea and the influence of sampling devices, *Aquatic Microbial*
937 *Ecology*, 58, 67-78, 2009.
- 938 Stramma, L., Johnson, G. C., Sprintall, J., and Mohrholz, V.: Expanding Oxygen-Minimum Zones
939 in the Tropical Oceans, *Science*, 320, 655-658, 2008.
- 940 Sugimura, Y. and Suzuki, Y.: A high-temperature catalytic oxidation method for the
941 determination of non-volatile dissolved organic carbon in seawater by direct injection of a liquid
942 sample, *Marine Chemistry*, 24, 105-131, 1988.
- 943 Tarazona, J. and Arntz, W.: The Peruvian Coastal Upwelling System. In: *Coastal Marine*
944 *Ecosystems of Latin America*, Seeliger, U. and Kjerfve, B. (Eds.), Ecological Studies, Springer
945 Berlin Heidelberg, 2001.
- 946 Upstill-Goddard, R. C., Frost, T., Henry, G. R., Franklin, M., Murrell, J. C., and Owens, N. J. P.:
947 Bacterioneuston control of air-water methane exchange determined with a laboratory gas
948 exchange tank, *Global biogeochemical cycles*, 17, 1108, 2003.
- 949 Verdugo, P., Alldredge, A. L., Azam, F., Kirchman, D. L., Passow, U., and Santschi, P. H.: The
950 oceanic gel phase: a bridge in the DOM-POM continuum, *Marine Chemistry*, 92, 67-85, 2004.
- 951 Wallace, G. T. and Duce, R. A.: Transport of particulate organic matter by bubbles in marine
952 waters 1, *Limnology and Oceanography*, 23, 1155-1167, 1978.
- 953 Wilson, T. W., Ladino, L. A., Alpert, P. A., Breckels, M. N., Brooks, I. M., Browse, J., Burrows, S.
954 M., Carslaw, K. S., Huffman, J. A., Judd, C., Kilthau, W. P., Mason, R. H., McFiggans, G., Miller, L.
955 A., Najera, J. J., Polishchuk, E., Rae, S., Schiller, C. L., Si, M., Temprado, J. V., Whale, T. F., Wong,
956 J. P. S., Wurl, O., Yakobi-Hancock, J. D., Abbatt, J. P. D., Aller, J. Y., Bertram, A. K., Knopf, D. A.,
957 and Murray, B. J.: A marine biogenic source of atmospheric ice-nucleating particles, *Nature*, 525,
958 234-238, 2015.
- 959 Wood, R., Mechoso, C. R., Bretherton, C. S., Weller, R. A., Huebert, B., Straneo, F., Albrecht, B.
960 A., Coe, H., Allen, G., Vaughan, G., Daum, P., Fairall, C., Chand, D., Gallardo Klenner, L.,
961 Garreaud, R., Grados, C., Covert, D. S., Bates, T. S., Krejci, R., Russell, L. M., de Szoeki, S.,
962 Brewer, A., Yuter, S. E., Springston, S. R., Chaigneau, A., Toniazzo, T., Minnis, P., Palikonda, R.,
963 Abel, S. J., Brown, W. O. J., Williams, S., Fochesatto, J., Brioude, J., and Bower, K. N.: The VAMOS
964 Ocean-Cloud-Atmosphere-Land Study Regional Experiment (VOCALS-REx): goals, platforms, and
965 field operations, *Atmos. Chem. Phys.*, 11, 627-654, 2011.
- 966 Wurl, O., Miller, L., Röttgers, R., and Vagle, S.: The distribution and fate of surface-active
967 substances in the sea-surface microlayer and water column, *Marine Chemistry*, 115, 1-9, 2009.
- 968 Wurl, O., Miller, L., and Vagle, S.: Production and fate of transparent exopolymer particles in the
969 ocean, *J. geophys. Res.*, 116, C00H13, 2011.
- 970 Yu, H. and Mou, S.-F.: Effect of temperature on the retention of amino acids and carbohydrates
971 in high-performance anion-exchange chromatography, *Journal of Chromatography A*, 1118, 118-
972 124, 2006.
- 973 Zhang, Z.: Studies on the sea surface microlayer II. The layer of sudden change of physical and
974 chemical properties, *Journal of Colloid and Interface Science*, 264, 148-159, 2003.

- 975 Zhang, Z., Liu, L., Wu, Z., Li, J., and Ding, H.: Physicochemical Studies of the Sea Surface
976 Microlayer: I. Thickness of the Sea Surface Microlayer and Its Experimental Determination, J.
977 Colloid Interface Sci., 204, 294-299, 1998.
- 978 Zhou, J., Mopper, K., and Passow, U.: The role of surface-active carbohydrates in the formation
979 of transparent exopolymer particles by bubble adsorption of seawater, Limnology and
980 Oceanography, 43, 1860-1871, 1998.
- 981
- 982

983 **Legends**

984
985 Figure 1: Maps of stations where sampling for sea surface microlayer (SML) and underlying
986 seawater (ULW) was conducted during the SOPRAN Meteor 91 cruise along the coastal
987 upwelling area off Peru in 2012.

988
989 Figure 2a, b: Surface water (1m depth) temperature ($^{\circ}\text{C}$) and wind speed (m s^{-1}) (b) during M91.

990
991 Figure 3: Direct relationship between surface water temperature and wind speed during M91
992 SML sampling, $p < 0.001$, $r = 0.58$, $n = 39$. Data in dotted rectangle were selected for analysis of
993 wind speed effects at similar temperatures, see figure 7.

994
995 Figure 4: Phyto- and bacterioneuston ($< 20 \mu\text{m}$) abundance (number mL^{-1}) in the SML off Peru
996 during M93: NCPL: ‘Non-cyanobacterial-type’ phytoplankton, CPL: ‘cyanobacterial-type’
997 phytoplankton, HPL: heterotrophic bacterioplankton.

998
999 Figure 5: Surface distribution patterns of organic matter concentrations in the SML during M91
1000 showing particulate organic carbon (POC, $\mu\text{mol L}^{-1}$), dissolved organic carbon (DOC, $\mu\text{mol L}^{-1}$)
1001 dissolved hydrolysable carbohydrates (DCCHO, nmol L^{-1}), dissolved hydrolysable amino acids
1002 (DHAA, nmol L^{-1}) and abundance of TEP (L^{-1}) and CSP (L^{-1}).

1003
1004 Figure 6: Box and whisker plot of enrichment factors (EF) calculated for various particulate and
1005 dissolved components during M91. Each box encloses 50% of the data with the median value of
1006 the variable displayed as a line. The bottom of the box marks the 25%, and the top the 75% limit,
1007 of data. The lines extending from the top and bottom of each box marks the 10% and 90%
1008 percentiles within the data set and the filled circles indicate the data outside of this range. For
1009 abbreviations, see text.

1010
1011 Figure 7a, b: Influence of wind speed (m s^{-1}) on the total area concentration of TEP ($\text{mm}^2 \text{L}^{-1}$) in
1012 the SML at all stations (a) and relationship between TEP enrichment factors (EF) and wind speed
1013 (m s^{-1}) for only those stations that showed similar sea surface temperature as indicated in figure 3.

1014 Filled dots indicated data from stations of similar sea surface temperature. Data in plot (a) were
1015 fitted by power law functions; the solid line represents all data, the dotted line represents data of
1016 similar sea surface temperature.

1017
1018 Figure 8a, b: Size frequency distribution of TEP (a) and CSP (b) observed during the M91 cruise
1019 for samples collected from the SML (open symbols) and in the ULW (filled symbols) at the
1020 stations with lowest wind speed of 0.6 m s^{-1} (triangles) and highest wind speed of 9.0 m s^{-1}
1021 (circles). Linear regression of $\log(dN/d(dp))$ versus $\log(dp)$ was fitted to the particles in the size
1022 range of $1.05 - 14.14 \text{ }\mu\text{m}$ ESD.

1023
1024 Figure 9: Spatial distribution of the slope ratio, δ^* , for TEP in the upwelling region off Peru
1025 during M91.

1026
1027
1028
1029

1030 **Tables**

1031

1032 Table 1: Hydrographic conditions encountered during SML sampling off Peru in 2012

1033 (M91). Data on air temperature, wind speed, global and UV radiation were obtained from

1034 the ship's DShip database for the time of sampling.

1035

1036

1037

1038

1039

1040

1041

1042

1043

1044

1045

1046

1047

1048

1049

1050

1051

1052

1053

1054

1055

1056

1057

1058

1059

1060

1061

1062

1063

1064

1065

1066

1067

1068

1069

1070

1071

1072

1073

1074

1075

1076

	Temperature (°C)	Salinity	Air temperature (°C)	Wind speed (m s ⁻¹)	Global Radiation (W m ⁻²)	UV Radiation (W m ⁻²)
average	19.25	34.87	19.67	5.66	570	37935
SD	1.70	0.50	0.89	2.14	366	23384
Min	15.91	32.02	17.30	0.60	10	0.812
Max	21.90	35.32	21.50	9.00	1103	71.10

1077
 1078 Table 2: Concentration of various organic components in the SML during M91, given as average
 1079 (avg.) and standard deviation (SD), as well as minimum (min) and maximum (max); n = number
 1080 of observations. For abbreviations see text.
 1081

	Unit	Avg.	SD	min	max	n
DOC	$\mu\text{mol L}^{-1}$	94	13	71	122	39
TOC	$\mu\text{mol L}^{-1}$	127	33	82	199	39
POC	$\mu\text{mol L}^{-1}$	33	25	2.3	96	39
TEP number	$\times 10^6 \text{ L}^{-1}$	19	15	1.8	63	39
TEP area	$\text{mm}^2 \text{ L}^{-1}$	100	106	6.9	408	39
DCCHO	nmol L^{-1}	1111	550	507	2668	39
PCCHO	nmol L^{-1}	1084	1300	41	5156	34
TN	$\mu\text{mol L}^{-1}$	16	4.9	8.7	28	39
TDN	$\mu\text{mol L}^{-1}$	12.5	4.0	7.7	25	39
PN	$\mu\text{mol L}^{-1}$	3.3	3.7	bd	16	39
CSP number	$\times 10^6 \text{ L}^{-1}$	118	72	19	311	39
CSP area	$\text{mm}^2 \text{ L}^{-1}$	1024	728	137	3051	39
FAA	nmol L^{-1}	151	104	49	531	37
DHAA	nmol L^{-1}	770	359	423	2017	30
PHAA	nmol L^{-1}	1176	774	208	3956	29
NCPL	$\times 10^3 \text{ mL}^{-1}$	45	53	5.4	300	35
CPL	$\times 10^3 \text{ mL}^{-1}$	27	35	3.7	193	35
Het. bacteria	$\times 10^4 \text{ mL}^{-1}$	195	206	3	854	36

1082
 1083
 1084
 1085
 1086
 1087
 1088
 1089
 1090
 1091
 1092
 1093
 1094
 1095

1096
 1097
 1098 Table 3: Correlation coefficients (r) between concentrations of various organic components in the
 1099 SML and their concentration in the underlying seawater (ULW), temperature (T, °C), and wind
 1100 speed (U, m s⁻¹) at the time of sampling. Correlations yielding significance level of $p < 0.01$ are
 1101 marked bold. For abbreviations see text. *: only 30 samples were analyzed for NCPL and CPL
 1102 from the ULW.

1103
 1104
 1105
 1106
 1107
 1108
 1109
 1110
 1111
 1112
 1113
 1114
 1115
 1116
 1117
 1118
 1119
 1120
 1121
 1122
 1123
 1124
 1125
 1126
 1127
 1128
 1129
 1130
 1131
 1132
 1133
 1134
 1135
 1136
 1137
 1138
 1139

SML	r_{ULW}	r_T	r_U	n
DOC	0.75	-0.04	0.06	39
TOC	0.79	-0.53	-0.35	39
POC	0.68	-0.67	-0.48	39
TEP number	0.51	-0.58	-0.69	39
TEP area	0.58	-0.65	-0.69	39
DCCHO	0.94	-0.44	-0.29	39
PCCHO	0.77	-0.59	-0.38	34
TDN	0.24	-0.18	-0.05	39
PN	0.59	-0.55	-0.43	39
CSP number	0.53	-0.04	0.15	39
CSP area	0.68	-0.36	-0.31	39
FAA	0.34	-0.34	0.19	37
DHAA	0.30	-0.47	-0.37	30
PHAA	0.56	-0.64	-0.53	29
NCPL	0.70*	-0,24	-0,21	35
CPL	0.90*	-0,21	-0,31	35
Het. bacteria	0.92	-0.33	-0.37	36

1140 Figures

1141

1142

1143

1144

1145

1146

1147

1148

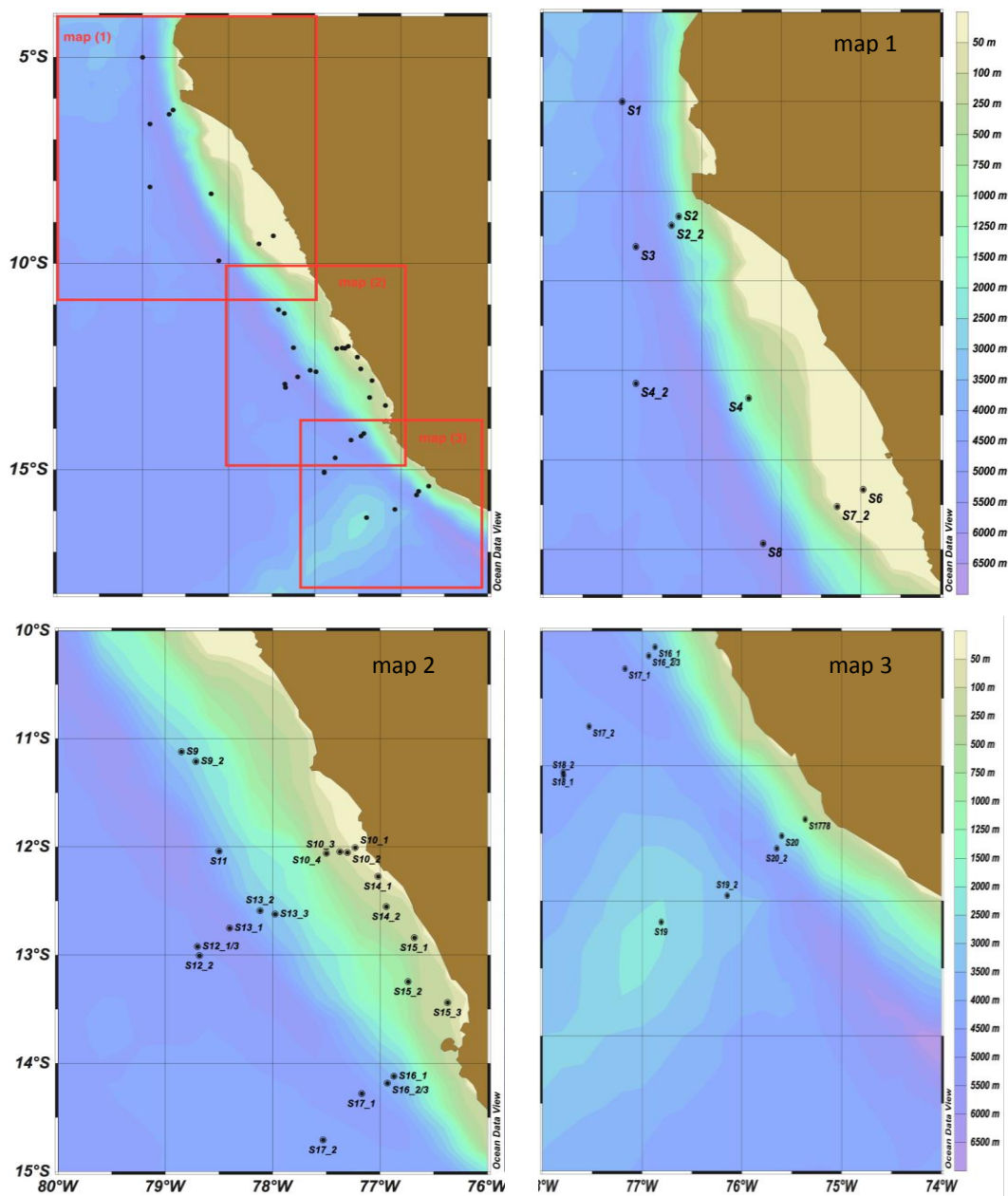
1149

1150

1151

1152

1153



1154

1155

1156

1157

1158

1159

1160

1161

1162

1163

1164

1165

1166

1167

1168

1169

Figure 1

1170
1171
1172
1173
1174
1175
1176
1177
1178
1179
1180
1181
1182
1183
1184
1185
1186
1187
1188
1189
1190
1191
1192
1193
1194
1195
1196
1197

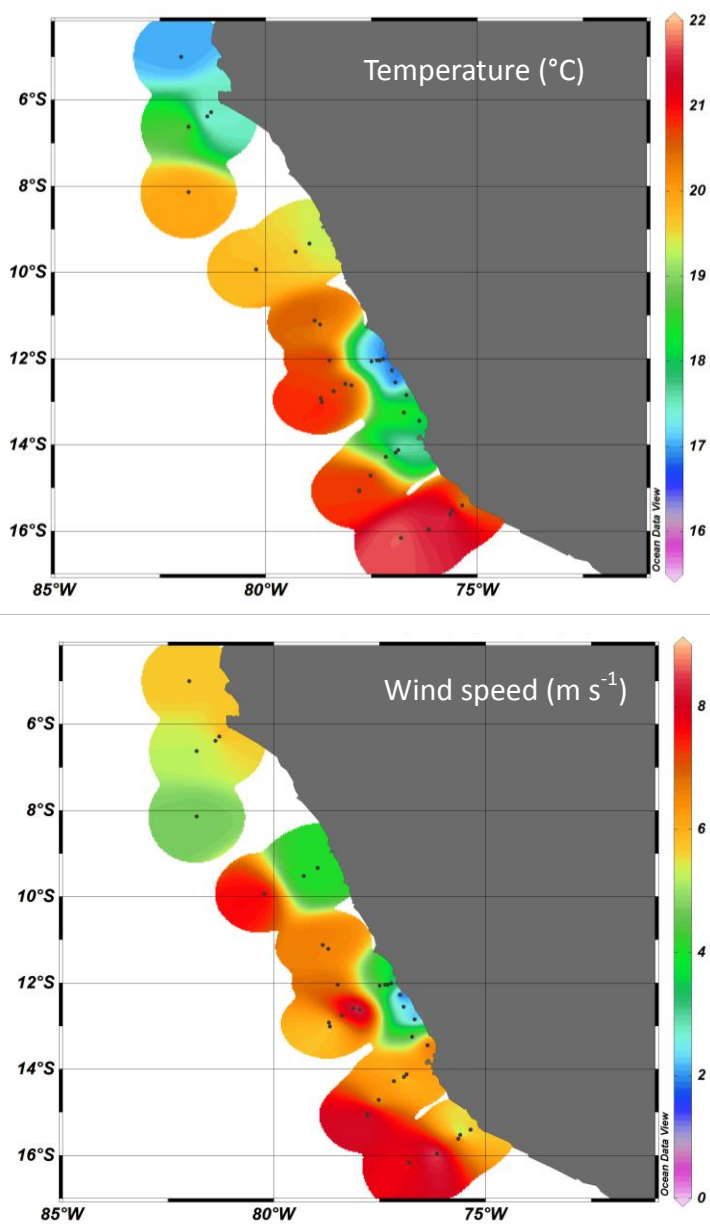
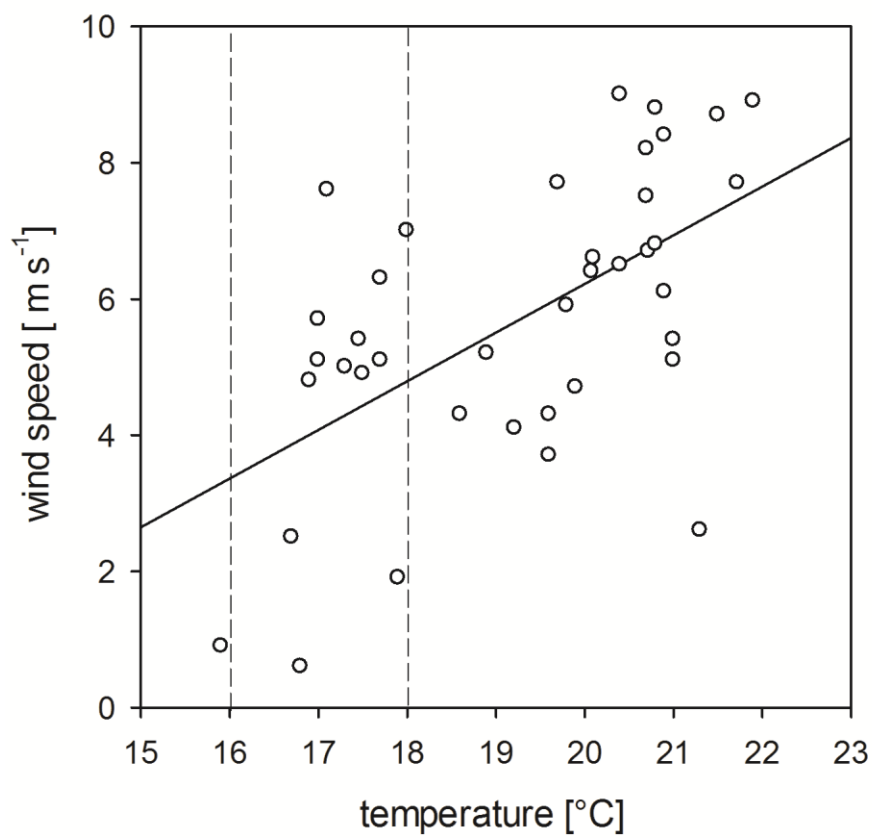


Figure 2



1198
1199
1200
1201
1202
1203
1204

Figure 3

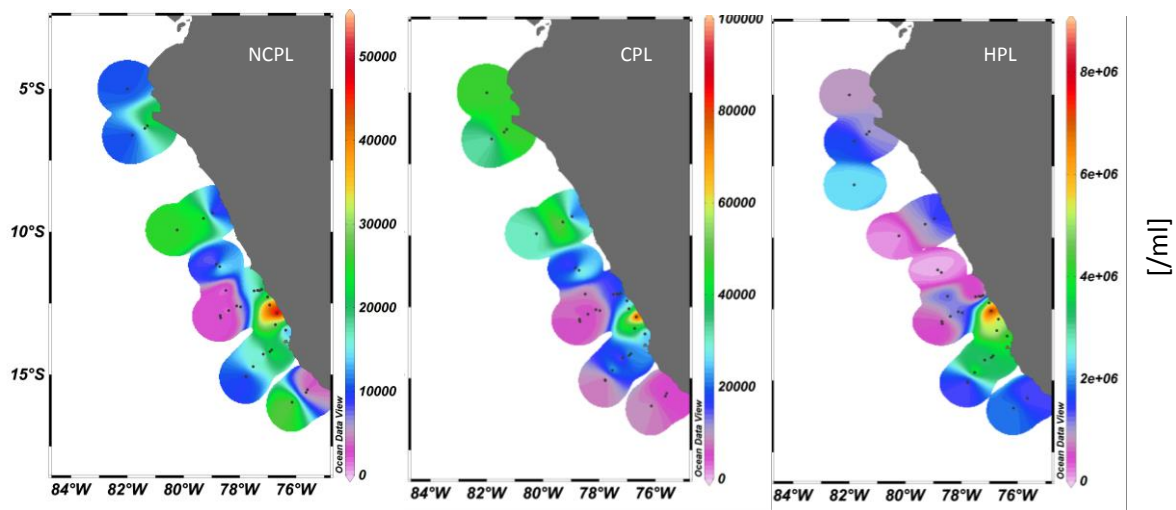
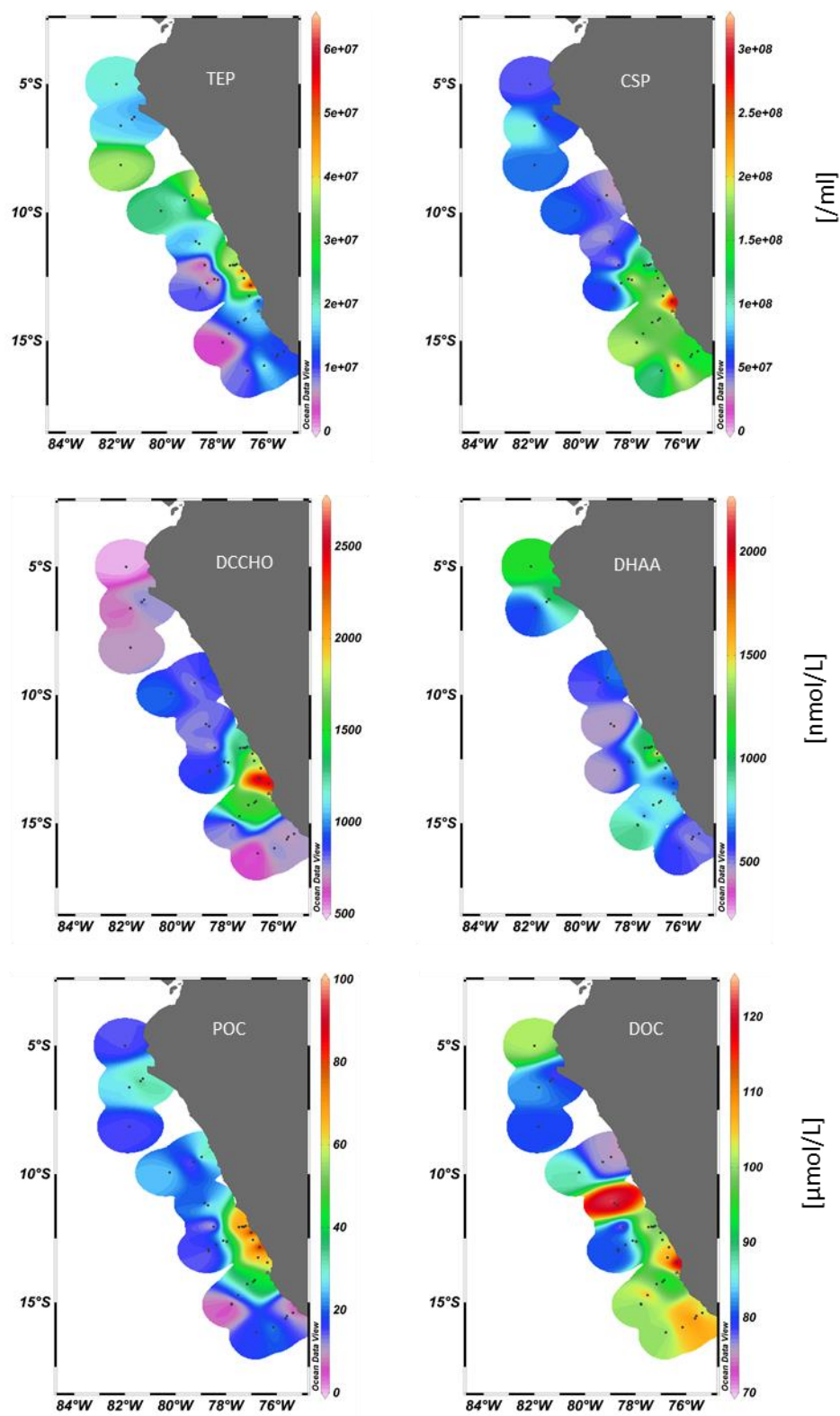


Figure 4

Figure 4

1243



1244
1245
1246
1247
1248

Figure 5

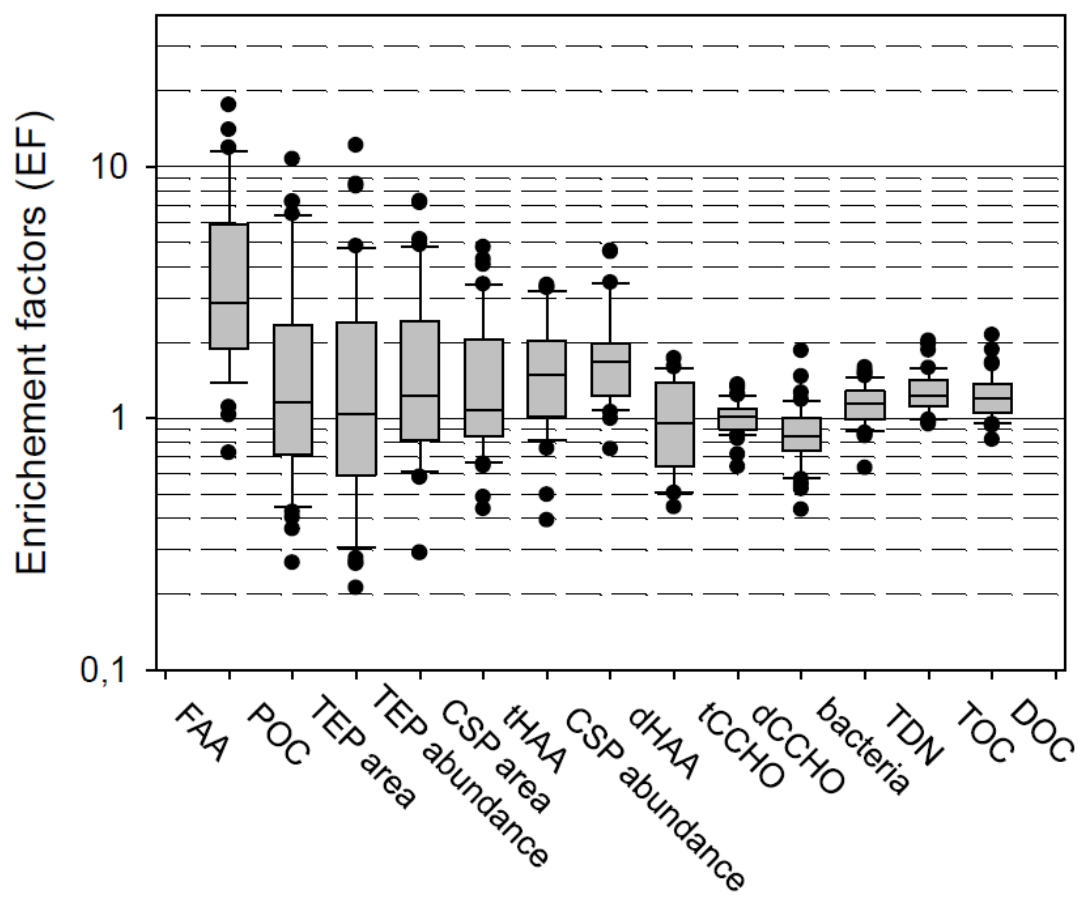


Figure 6

1249

1250

1251

1252

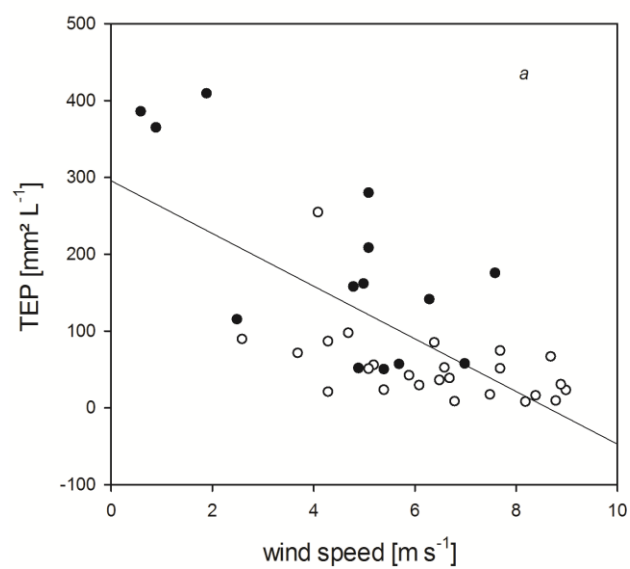
1253

1254

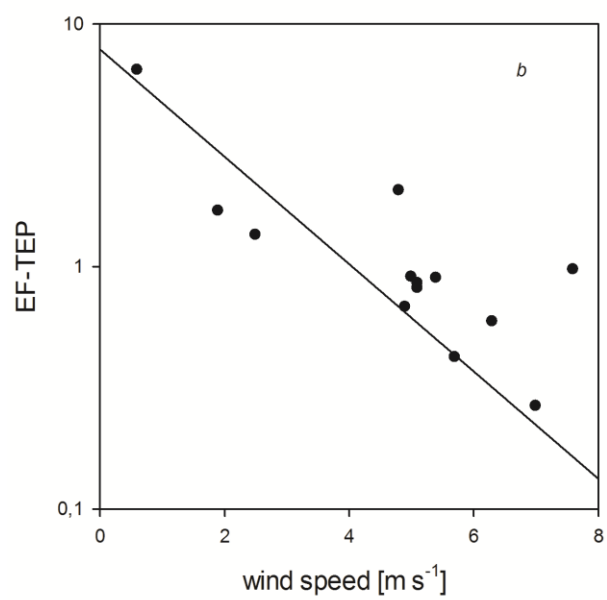
1255

1256

1257



1258



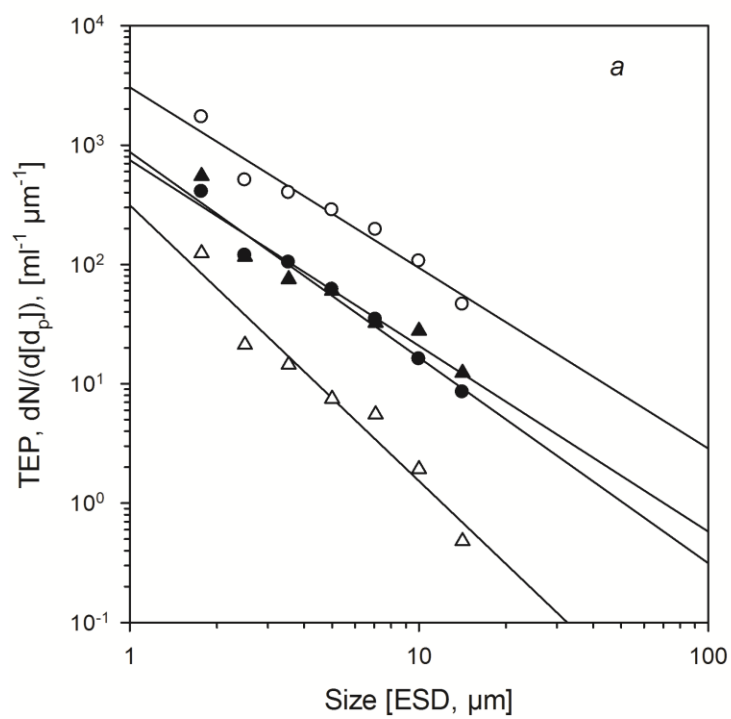
1259

1260

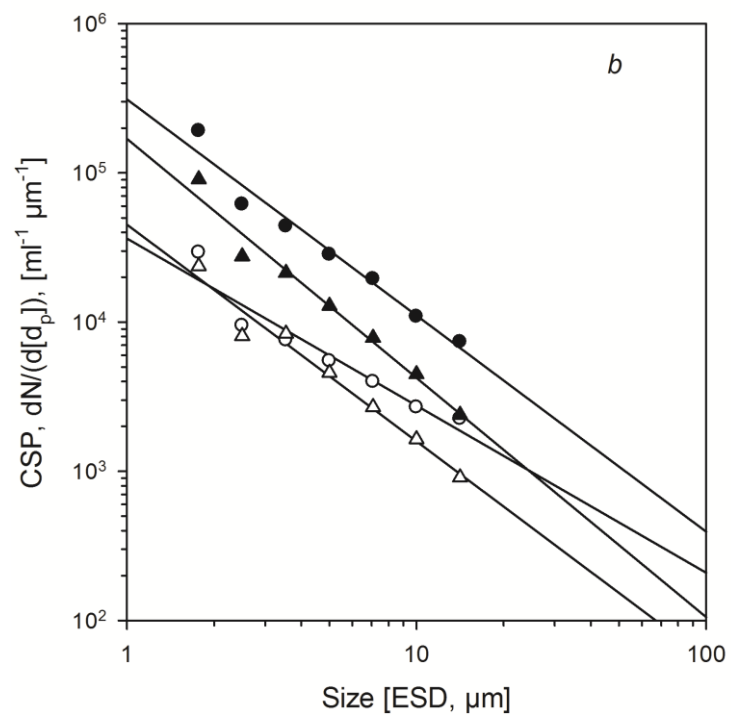
1261

1262

Figure 7a, b



1263



1264

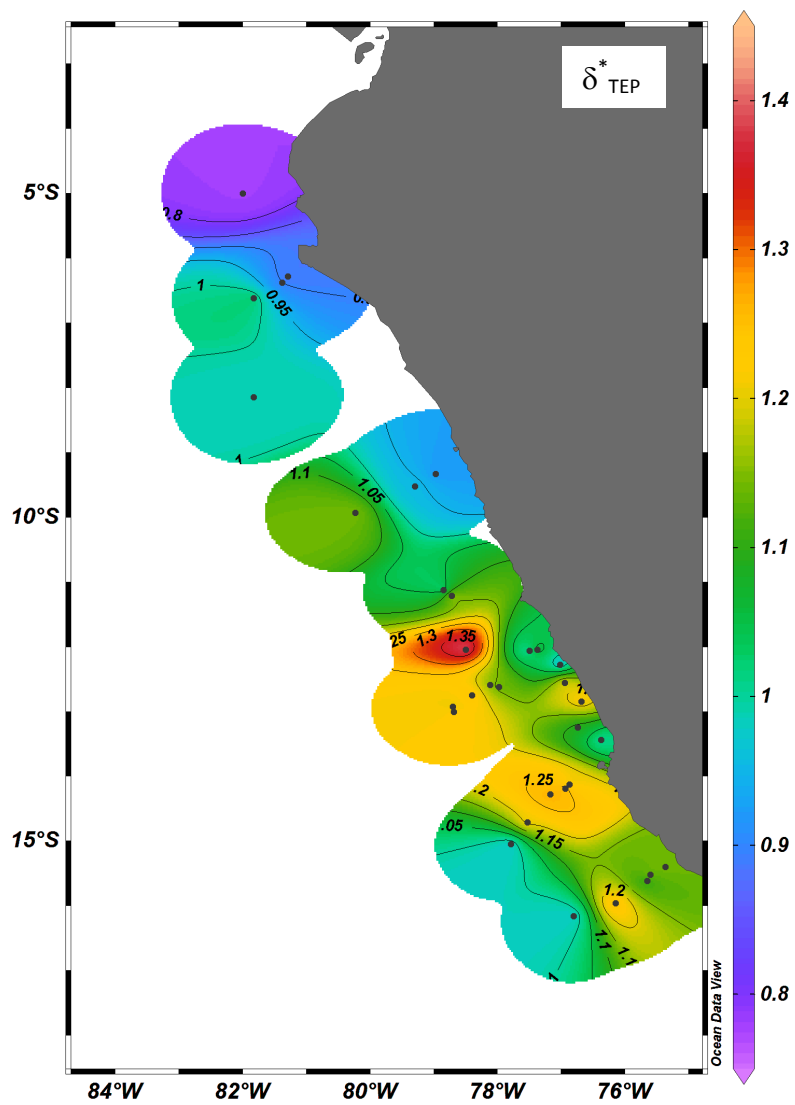
1265

1266

1267

1268

Figure 8a, b



1269

1270

1271

1272

Figure 9